

NASA Contractor Report 182064

**CONCEPTS AND ANALYSIS FOR PRECISION SEGMENTED
REFLECTOR AND FEED SUPPORT STRUCTURES**

**Richard K. Miller,
Mark W. Thomson and
John M. Hedgepeth**

**ASTRO AEROSPACE CORPORATION
Carpinteria, California**

**Contract NAS1-18567
December 1990**

(NASA-CR-182064) CONCEPTS AND ANALYSIS FOR
PRECISION SEGMENTED REFLECTOR AND FEED
SUPPORT STRUCTURES Final Report (Astro
Aerospace Corp.) 90 p CSCL 22B

N91-15300

Unclas

63/18 0329534



National Aeronautics and
Space Administration

Langley Research Center
Hampton, Virginia 23665-5225

1

2

3

4

5

6

7

8

9

10

TABLE OF CONTENTS

SECTION 1:	INTRODUCTION.....	1
SECTION 2:	ANALYSIS OF PROJECTED FLIGHT SUPPORT STRUCTURES	3
	2.1 Deployment Analysis of a Doubly Curved Pactruss.....	3
	2.1.1 Deployment of Pactruss Designs with Extensions	3
	2.1.2 Deployment of a Truss without Circumferentials	5
	2.1.3 Redundancy Reduction of Five-Ring Trusses	5
	2.1.4 Effect of Strut Fabrication Imperfections on Surface Error.....	6
SECTION 3:	DEPLOYABLE SUNSHADE CONCEPT.....	7
SECTION 4:	PRELIMINARY DESIGN OF A FEED SUPPORT STRUCTURE	8
	4.1 Cantilever Configuration	8
	4.1.1 Fundamental Frequency of Vibration.....	9
	4.1.2 Block Area Ratio	10
	4.1.3 Structural Mass Ratio.....	10
	4.1.4 Parametric Results.....	11
	4.1.5 Required Minimum Shear Modulus	12
	4.1.6 Comments on Lattice Beam.....	13
	4.2 Rim-Tripod Configuration.....	13
	4.2.1 Fundamental Frequency of Vibration of Individual Struts	14
	4.2.2 Fundamental Frequency of Vibration for Rotation of Feed Device About Any Strut Axis	17
	4.2.3 Fundamental Frequency of Vibration for Vertical Translation of Feed Device	17
	4.2.4 Block Area Ratio.....	18
	4.2.5 Structural Mass Ratio.....	18
	4.2.6 Parametric Studies.....	19
	4.3 Sunshade-Tripod Configuration.....	20
	4.3.1 Fundamental Frequency of Vibration of Individual Struts	20
	4.3.2 Fundamental Frequency of Vibration for Rotation of Feed Device About Any Strut Axis	21
	4.3.3 Fundamental Frequency of Vibration for Vertical Translation of Feed Device	21
	4.3.4 Blocked Area Ratio.....	22
	4.3.5 Structural Mass Ratio.....	22
	4.3.6 Parametric Studies.....	22
	4.4 Radial Spoke Bicycle Wheel Configuration.....	23
	4.4.1 Required Wire Tensile Stress.....	24



TABLE OF CONTENTS, Continued

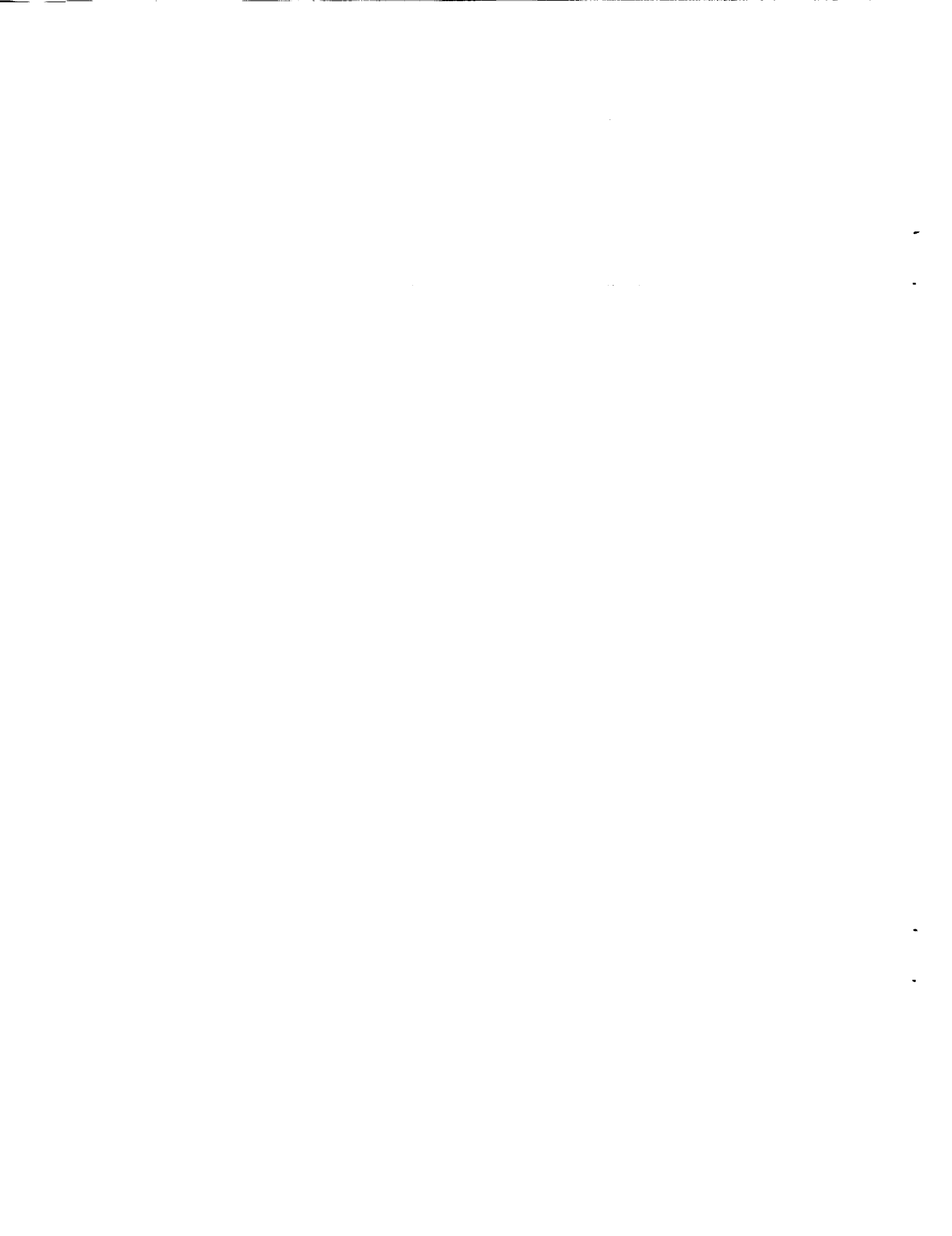
4.4.2	Fundamental Frequency of Vibration for Vertical Translation of Feed Device.....	25
4.4.3	Fundamental Frequency of Vibration for Pure Rocking of the Feed About an Axis Normal to the Reflector Axis.....	27
4.4.4	Fundamental Frequency of Vibration for Pure Torsion of the Feed About the Reflector Axis.....	29
4.4.5	Blocked Area Ratio.....	30
4.4.6	Structural Mass Ratio.....	31
4.4.7	Parametric Studies.....	31
4.5	Interlaced Spoke Bicycle Wheel Configuration.....	33
4.5.1	Required Spoke Tensile Stress.....	33
4.5.2	Fundamental Frequency of Vibration for Vertical Translation of Feed Device.....	34
4.5.3	Fundamental Frequency of Vibration for Pure Rocking of the Feed about an Axis Normal to the Reflector Axis.....	34
4.5.4	Fundamental Frequency of Vibration for Pure Torsion of the Feed about the Reflector Axis.....	35
4.5.6	Structural Mass Ratio.....	37
4.5.6.1	Added Rim Mass Due to Included Rim Compression.....	37
4.5.6.2	Total Structural Mass Ratio.....	40
4.5.7	Parametric Studies.....	41
4.6	Conclusions for Preliminary Design of a Feed Support Structure.....	41
SECTION 5:	CONCLUSIONS.....	43
REFERENCES:	44
ABSTRACT:	REPORT DOCUMENTATION PAGE.....	85

LIST OF TABLES AND FIGURES

TABLE 3-1:	RESULTS OF MONTE CARLO RUNS	45
TABLE 4-1:	RESTORING MOMENT CREATED BY INDIVIDUAL WIRES FOR ROTATIONS SHOWN IN FIGURE 4-13 FOR RSBW CONFIGURATION	46
TABLE 4-2:	COMPARISON OF DESIGN PARAMETERS FOR 10 HZ FEED SUPPORT STRUCTURES OF VARIOUS CONFIGURATIONS	47
Figure 1-1.	Design to avoid pop-through.....	48
Figure 2-1.	Application of Pactruss to LDR.....	49
Figure 2-2.	Pactruss concept	50
Figure 2-3.	Triangular Pactruss	51
Figure 2-4.	Hybrid Pactruss	52
Figure 2-5.	Parts of hybrid Pactruss.....	53
Figure 2-6.	XGTEST	54
Figure 2-7.	Design to avoid pop-through.....	55
Figure 2-8.	XGTK.....	56
Figure 2-9.	HEXPAK.....	57
Figure 2-10.	Deployment angle of outer bay.....	58
Figure 2-11.	Deployment analysis model for the case without circumferentials	59
Figure 2-12.	Deployment without circumferentials, outer bay drive.....	60
Figure 2-13.	Deployment sequence for model without circumferentials.....	61
Figure 2-14.	Five-ring tetrahedral truss	62
Figure 2-15.	Five-ring Pactruss.....	63
Figure 2-16a.	Tetrahedral truss upper surface.....	64
Figure 2-16b.	Tetrahedral truss lower surface	65
Figure 2-17.	Simplified Pactruss	66
Figure 3-1.	Deployable support truss and sunshade	67
Figure 4-1.	Cantilever configuration of feed support structure	68
Figure 4-2.	Feed support mass ratio μ versus assigned values of blocked area ratio, "a", fundamental vibration frequency, f_n , and radius of gyration, r_g , for the cantilever configuration	69
Figure 4-3.	Effect of radius of gyration of feed mass on required mass ratio μ for fixed natural frequency and blocked area ratio.....	70
Figure 4-4.	Minimum required G_{eff}/E to guarantee that f_n - torsion $\geq f_n$ - bending for the cantilever configuration.....	71
Figure 4-5.	Rim-tripod configuration of feed support structure	72

LIST OF TABLE AND FIGURES, Continued

Figure 4-6.	Rim-tripod FSS geometry - planar view through a single strut and reflector axis for the case $F/D = 0.5$ and $D = 20$ m	73
Figure 4-7.	Planar view of tripod FSS with plane determined by centerlines of struts AB and AC. Axis of rotation is centerline of AB.....	74
Figure 4-8.	Feed support structure mass ratio (μ) versus assigned values of blocked area ratio, "a," fundamental f_n , and radius of gyration r_g , for the rim tripod configuration.....	75
Figure 4-9.	Sun shade-tripod configuration of feed support structure	76
Figure 4-10.	Sun shade-tripod FSS geometry - planar view through a single strut and reflector axis for the case $F/D = 0.5$ and $D = 20$ m.....	77
Figure 4-11.	Structural mass ratio versus blocked area ratio for sunshade tripod configuration	78
Figure 4-12.	Radial spoke bicycle wheel configuration	79
Figure 4-13.	Geometry of pure rotation of feed device about an axis (Z) normal to reflector axis for RSBW configuration.....	80
Figure 4-14.	Geometry of torsional deformation of feed device about an axis (Z) normal to reflector axis for RSBW configuration.....	80
Figure 4-15.	Dependence of fundamental frequency, f_n , for rocking vertical translation and torsion as functions of blocked area, "a," and mass ratio, μ , radial spoke bicycle wheel configuration	81
Figure 4-16.	Interlaced spoke bicycle wheel (ISBW) configuration.....	82
Figure 4-17.	Geometry of deformation of spoke AB during torsional motion, ISBW configuration.....	83
Figure 4-18.	Fundamental frequency versus blocked area ratio and structural mass ratio for ISBW configuration	84



SECTION 1

INTRODUCTION

The Precision Segmented Reflector (PSR) project is a step towards developing the technology base needed to support future advanced astrophysics missions. The focus of the project is to develop a lightweight, low-cost option for utilizing large reflecting telescopes that can be assembled or deployed in space.

The goal of PSR structures development is to demonstrate doubly curved truss concepts and geometries suitable for space deployment or assembly that will properly support the composite reflector panels that are under development. The specific objectives and goals of the development are to achieve:

- 1) Structure areal density of 5 kg per meter square
- 2) Initial deployment or assembly accuracy of 100 micrometers
- 3) Dimensional stability of 100 micrometers in a typical mission orbital thermal environment
- 4) Micron level dynamic simulation capability
- 5) Micron level structural testing and characterization capability.

Several prior bodies of research have contributed to the work reported herein. In Reference 1, the Pactruss concept was studied for application to precision, doubly curved, parabolic reflectors such as PSR and the Large Deployable Reflector (LDR). Geometric requirements for the Pactruss were defined and computer programs were written that will generate such geometry for any parabolic/truss configuration. Structural performance for a specific design was then characterized statically, dynamically, and as a function of truss depth. Finally, deployment analyses of the chosen configuration were conducted. To achieve deployment without strain or structural lockup, the truss surface shape was designed as a series of annular regions, alternating between flat and sloped areas. Short strut extensions in the valley of each pair of annuli were required to maintain the specified parabolic shape at the truss surface nodes (see Figure 1-1).

The Pactruss was found to be capable of enough precision and stiffness to support the PSR reflector panels, stow around a central body for launch, permit ground-based testing with small distortion in one g and deploy in a strain-free manner.

In Reference 2, networks of truss beams for proposed Space Station structures were studied for distortions resulting from expected manufacturing, testing, assembly and operational influences. Structural characteristics were defined and a model was analyzed for behavior during thermal gradients, assembly operations, and as a result of random manufacturing imperfections. Published algorithms and appropriate methods for analysis of random errors were reviewed. Appropriate software and analytical methods were developed. The methods developed are able to generate data on overall deflection and cumulative geometric errors, residual stresses, and misalignment of reference planes in multiple element truss structures due to random member length errors.

An essential part of the LDR structural configuration is a tubular shroud needed to prevent sunlight from striking the cold primary and secondary mirror. Also required is a structure connecting the primary and secondary mirrors. Concepts for both of these systems are reported herein.

Further analysis of Pactruss deployment has been undertaken to attempt to minimize the lock-up phenomena identified in Reference 1 for a Pactruss without extensions. A study of the effects of fabrication errors on deployable and erectable PSR trusses using the aforementioned methods was undertaken. The effects of reducing the number of components in a deployable LDR-type Pactruss were evaluated. Design studies for deployment actuation concepts for large PSR trusses were generated.

SECTION 2

ANALYSIS OF PROJECTED FLIGHT SUPPORT STRUCTURES

As discussed in the introduction, a flight mission that will require PSR technology is a large infrared astronomical observatory utilizing the Large Deployable Reflector (LDR). Application of the Pactruss concept to this mission is depicted in Figure 2-1. The basic Pactruss structure stows by alternately raising one row of central vertical members and lowering the adjacent row while synchronously collapsing all rows lengthwise as shown in Figure 2-2. A model of a Pactruss with triangularly oriented rows is shown stowed, partially deployed and deployed in Figure 2-3.

For application to LDR, the precise geometry of 20-meter-diameter, five-ring hybrid Pactruss was generated. The hybrid truss was conceived because of the requirement that the truss stow around a central body which would house optical or cryogenic equipment for the infrared astronomy mission (see Figure 2-4). The hybrid is comprised of Pactruss pie-segments which fit between single-fold beams. While the Pactruss segments stow in two directions, the beams stow only along their length, thus producing a ring of stowed members around the fixed inner members of the beams which are arrayed in a hexagon. This is clearly depicted in Figure 2-5.

2.1 DEPLOYMENT ANALYSIS OF A DOUBLY CURVED PACTRUSS

To study deployment performance, a portion of the test bed hybrid Pactruss geometrical model was analyzed with ASTRAN, a high-fidelity structural deployment analysis program (see Reference 6). As reported in Reference 3, the straightforward model exhibited a serious deployment defect. Although the inner bay deployed easily, the outer ones only partly deployed, ending in the position shown in Figure 2-6. The solution to the problem was found to be to design the truss so that the downward-stowing members never pass through the horizontal plane. This yields a stepped truss to which extensions must be added for the parabolic reflector support point as shown in Figure 2-7.

Two versions of this approach as applied to the two-ring test-bed structure are shown in Figures 2-8 and 2-9. In Figure 2-8, the XGTK has the outer bay horizontal, and was shown in Reference 3 to deploy smoothly. In order to reduce the length of the extensions, the alternative configuration called HEXPAK, Figure 2-9, was created. In

this configuration, the inner ring stows downward and thus never deploys past the horizontal.

2.1.1 Deployment of Pactruss Designs With Extensions

The partial test bed model, HEXPAK, was modeled using ASTRAN for deployment performance. The results are compared with those for XGTEST and XGTK previously obtained and shown in Figure 2-10. Deployment of XGTEST was unsuccessful as previously mentioned due to the pop-through problem. A maximum of 10 Nm deployment movement was applied at the inner, bottom members. The XGTK configuration was analyzed for 0, 1.0 and 10.0 Nm drive movements. The HEXPAK was shown to require no significant deployment moment and thus produced no strain in the members.

2.1.2 Deployment of a Truss Without Circumferentials

The preceding configurations exhibiting satisfactory deployment behavior have the disadvantage of requiring extensions, with the attendant increase in complexity. Another approach would be to remove the constraint caused by the circumferentials. For this reason, a deployment analysis was performed for the segment without circumferentials shown by the solid lines in Figure 2-11. Since the model has a relatively small number of degrees of freedom, the analysis proceeded rapidly. The important results are shown in Figures 2-12 through 2-17.

In all cases, complete deployment was achieved with no serious difficulties. In all cases, however, some straining of the members is necessary to overcome geometric constraints. The standard "level-hinge" arrangement consists of hinge lines parallel to the length-width directions in the truss. The necessary amount of drive moment, shown by the curve labeled "Level Hinges," is negative for the first two-thirds of deployment. The hinge drive acts to retard deployment which is being driven by springs in the diagonal knee hinges. When the longerons reach their maximum allowed separation, they begin to bend as deployment proceeds. The drive moment then goes positive to produce the bending. After the longerons reach their maximum bending, they relax, powering the deployment to completion.

Schematic illustrations of the truss during deployment are shown in Figure 2-13. The bending is too small to be seen in the illustration.

To reduce the amount of strut distortion, the hinges were slanted so that the longeron separation was monotonically increasing during deployment. The resulting driving moment, shown in Figure 2-12 by the curve labeled "Overslanted Hinges," immediately begins to climb to a value as large as that seen for the level hinges. In this instance, the diagonals are being distorted to accommodate the new geometry. No longeron bending is needed, but a driving moment is required to strain the diagonals.

A better design incorporates a moderate amount of hinge slanting. The diagonals strain during the initial part of deployment, but not very much, and the longerons strain during the latter part, but not very much. As seen in Figure 2-12, the relaxing diagonals provide the power to drive the deployment to completion during the second half.

The results indicate that good deployment behavior can be obtained with a reduced member Pactruss without extensions if the circumferentials are omitted.

2.1.3 Redundancy Reduction of Five-Ring Trusses

The five-ring tetrahedral and Pactruss structures shown in Figures 2-14 and 2-15 were modified for reduced complexity and enhanced deployment capability in the case of the Pactruss (see the preceding section).

In Figures 2-16 a and b, the modifications to the tetrahedral or Tetratruss are depicted. The removal of 201 struts reduces this design to static determinacy.

Figure 2-17 depicts the reduced member Pactruss. Although it was not possible to achieve static determinacy with this configuration and retain the ability to deploy, 72 percent of the redundants were eliminated. Only the most lightly loaded members were affected.

In reduction of the tetrahedral truss to static determinacy, the overall structural stiffness was reduced by a factor of four. The reason for this large reduction is not obvious and is left for future investigation. However, similar results were reported in Reference 5 for rectangular planar trusses.

2.1.4 Effect of Strut Fabrication Imperfections on Surface Error

A Monte Carlo analysis of the effects of random errors in member lengths for deployable and erectable trusses was performed using methods developed in Reference 2. The results of all Monte Carlo analyses are summarized in Table 2-1. They indicate that the Pactruss and the tetrahedral truss configurations exhibit nearly the same sensitivity to tolerances. Also, in both designs, the removal of redundant members increases the sensitivity. In the case of the Pactruss, the removal of circumferential members approximately doubled the sensitivity. For the tetratruss, the removal of enough members to make the truss statically determinate quadrupled the tolerance sensitivity.

The conclusion from these studies is that reducing the truss redundancy is an option that can be considered in design. The reduction has the advantage of simplicity, less erection time, or simplified deployment. The disadvantage is a significant loss of stiffness.

SECTION 3

DEPLOYABLE SUNSHADE CONCEPT

A deployable sunshade (shroud) concept was developed and is shown in Figure 3-1. This design is capable of stowing and deploying synchronously with the Pactruss design. The long upright members in the figure do not fold for stowage, so the package length is increased by the shroud length.

SECTION 4

PRELIMINARY DESIGN OF A FEED SUPPORT STRUCTURE

Reported herein are the results of preliminary design studies for a structure to support the feed device at the focus of a 20-meter parabolic reflector with $F/D = 0.5$. Since the intended application for the reflector is that of an orbiting telescope, the reflector is attached at its rim to a 20-meter-diameter, cylindrical sunshade structure, concentric with the reflector axis, and extending beyond the feed device. The presence of this sunshade structure is used to advantage in some of the structural configurations considered herein.

While many criteria may be selected to guide the development and evaluation of the feed support structure, we focused on three fundamental features: (1) the lowest natural frequency of vibration, (2) the fraction of the reflector frontal area which is shaded by the feed support structure, and (3) the mass of the support structure. Several configurations were examined using these criteria, and the results are reported in the following sections. In all cases, the feed was assumed to be a 300 kg cylinder of length 1.5 meters and diameter 1.5 meters. The radius of gyration of the feed was assumed to be 0.5 meter. The reflector and sunshade were assumed to be rigid at all desired attachment points with the feed support structure. Furthermore, all designs assume that the feed support structure is made of a material with $E = 227.5 \times 10^9 \text{ N/m}^2$ and $\rho = 1740 \text{ kg/m}^3$.

4.1 CANTILEVER CONFIGURATION

One of the simplest concepts for the feed support structure (FSS) is that of a single boom, cantilevered from the rim and extending upward in a straight line to the feed device. A schematic of this configuration is shown in Figure 4-1. It is assumed that the attachment at the rim is essentially rigid, so that the structural action of the boom is that of a simple cantilever beam.

Although there are a variety of approaches that may be chosen for configuring this beam, perhaps the simplest is that of a continuous hollow cylinder. This thin-walled cylinder approach is pursued next in order to provide a few quantitative measures of the merit of this configuration.

4.1.1 Fundamental Frequency of Vibration

The simple cantilever beam with tip-mass as shown in Figure 4-1 has a bending frequency which may be approximated as

$$f_n = \frac{1}{2\pi} \left(\frac{3EI/\ell^3}{M_{feed}} \right)^{\frac{1}{2}} \left[1 + \frac{9}{4} \left(\frac{r_g}{\ell} \right)^2 + 0.236 \frac{m\ell}{M_{feed}} \right]^{-\frac{1}{2}} \quad (1)$$

where

E	$= 227.5 \times 10^9 \text{ N/m}^2$	$=$ Modulus of elasticity
I	$\equiv \pi r^3 t$	$=$ Moment of inertia of cylinder
ℓ	$= 12.5 \text{ m}$	$=$ Length of beam
M_{feed}	$= 300 \text{ kg}$	$=$ Mass of feed device at tip
r_g	$= 0.5 \text{ m}$	$=$ Radius of gyration of feed device
m	$= 2 \pi r t$	$=$ Mass/length of beam
ρ	$= 1740 \text{ kg/m}^3$	$=$ Mass density of beam material

(2)

Equation (1) may be derived from Rayleigh's Principle assuming a mode shape equal to the static deflection shape $\phi(x)$ of a cantilever beam with a concentrated tip load.

$$\phi(x) = -\frac{1}{2} \left(\frac{x}{\ell} \right)^3 + \frac{3}{2} \left(\frac{x}{\ell} \right)^2 \quad (3)$$

The fundamental frequency of vibration of the beam will be the bending frequency given by equation (1), unless the effective shear modulus of the material is so small that the torsional frequency governs. As discussed in a later section, the approach taken here is that the bending frequency shall govern by intentional design of the beam. We later investigate the required effective shear modulus to meet this requirement. Hence, it is assumed that the fundamental frequency of vibration is given by equation (1).

4.1.2 Blocked Area Ratio

Another feature of the FSS performance is the amount of frontal area of the reflector surface which it shades. Since the shaded region of the reflector is rendered useless, it is naturally desired to minimize this "blocked" or shaded area. The cantilever beam produces a blocked area of

$$A_{\text{block}} = (2r)(9.25m) = (18.5m) r \quad (4)$$

While the total frontal area of the reflector is

$$A_{\text{frontal}} = \pi (10m)^2 = 314.2m^2 \quad (5)$$

A convenient nondimensional measure of the detrimental effects of blocked area is provided by the blocked area ratio, a , where in this case

$$a = \frac{A_{\text{block}}}{A_{\text{frontal}}} = (0.0589/m) r \quad (6)$$

Equivalently, the beam radius r may be expressed in terms of the blocked area ratio a as

$$r = (17.0m) a \quad (7)$$

4.1.3 Structural Mass Ratio

As in all space-borne structural applications, the mass of the structure, in this case the FSS, is an important parameter. For the thin-walled cylindrical beam proposed here, the mass M_{FSS} of the feed support structure is given by

$$M_{\text{FSS}} \equiv 2\pi r t \ell \rho = 2\pi (12.5 m)(1740 \text{ kg/m}^3) r t \quad (8)$$

A convenient nondimensional measure of the detrimental effects of structural mass is provided by the structural mass ratio μ where

$$\mu = \frac{M_{\text{FSS}}}{M_{\text{feed}}} = \frac{M_{\text{FSS}}}{300 \text{ kg}} \quad (9)$$

Substituting equation (8) into (9) leads to the expression

$$\mu = (456/m^2) rt \quad (10)$$

4.1.4 Parametric Results

By substituting from equations (7) and (10) into equation (1), and using the available numerical values from equations (2), it is possible to obtain a single relation between f_n , μ and a . This parametric relation may be written as

$$\mu = \frac{1 + \frac{9}{4} \left(\frac{r_g}{\ell} \right)^2}{\left(\frac{242 \text{ Hz}}{f_n} \right)^2 a^2 - 0.236} \quad (11)$$

Equation (11) may be used to investigate the required structural mass ratio μ for an FSS with assigned values for blocked area ratio a fundamental vibration frequency f_n and radius of gyration r_g . Shown in Figure 4-2 are the results of such parametric studies. Specifically, three curves are presented for designs with fundamental vibration frequencies of 5 Hz, 10 Hz, and 20 Hz, in the special case where $(r_g/\ell) = 0$. These curves generally fall from upper left to lower right, and demonstrate that

- (1) A small blocked area ratio requires a high structural mass ratio.
- (2) A high fundamental vibration frequency requires a high structural mass ratio.

Also shown in Figure 4-2 are contours for fixed values of cylinder radius r and thickness t . Equations for these curves may be obtained from equations (7) and (10). The contours together with the performance curves previously described may be used to estimate all major features of the beam design. For example, consider a beam with a required fundamental vibration frequency of 10 Hz, and a minimum wall thickness of 1 mm. It is shown in Figure 4-2 that the minimum weight FSS, which satisfies these requirements, has a structural mass ratio of about 46 percent, and a blocked area ratio of about 6.4 percent. Furthermore, the resulting beam has a radius of about 1 m and a wall thickness of 1 mm.

The effects of a non-zero radius of gyration r_g of the feed device are shown in Figure 4-3. Since this effect enters equation (11) in a simple multiplicative fashion, all

results may be expressed by a single curve. Note that for the assumed baseline parameter $r_g = 0.5$ and $\ell = 12.5$ m, the required increase in structural mass ratio μ for all cases is only 0.36 percent, and is therefore negligible. Hence, the results presented in Figure 4-2 may be used directly for the baseline configuration.

4.1.5 Required Minimum Shear Modulus

The cantilever configuration may have a fundamental vibration frequency which is governed by torsion, if the effective shear modulus of the composite cylindrical beam is too low. However, it is very difficult to estimate this effective modulus G , since it depends on the details of the diagonal wrap plies. The approach adopted herein is to require the effective shear modulus to be sufficiently large that the bending frequency governs for all designs. Presented next is an analysis of the required ratio of effective shear modulus G to the effective modulus of elasticity (E) for the cylindrical beam. The fundamental torsional frequency of the beam may be estimated as

$$f_n = \frac{1}{2\pi} \sqrt{\frac{G_{\text{eff}} J}{\left(I_{\text{feed}} + \frac{I_{\text{beam}}}{3} \right) \ell}} \quad (12)$$

where

$$\begin{aligned} G_{\text{eff}} &= \text{Effective shear modulus of cylindrical beam} \\ J &= \text{Polar moment of inertia of area of cylindrical beam} \cong 2\pi r^3 t \\ I_{\text{feed}} &= \text{Mass moment of inertia of feed device} = M r_g^2 \\ I_{\text{beam}} &= \text{Mass moment of inertia of cylindrical beam} \cong J \ell \rho \end{aligned} \quad (13)$$

Substituting from equations (7) and (10), and (13) into (12), the torsional frequency may be written in terms of G_{eff} , μa , and (r_g/ℓ) . A similar expression for the fundamental bending frequency may be obtained from equation (11). Solving these equations for G_{eff} , and E , respectively, and taking the ratio, the requirement that the torsional frequency always equals or exceeds the bending frequency may be expressed as

$$\frac{G_{\text{eff}}}{E} \geq (09.22) \frac{\mu a^2 \left[1 + \frac{1.62 \left(\frac{r_g}{\ell} \right)^2}{\mu a^2} \right]}{1 + \frac{9 \left(\frac{r_g}{\ell} \right)^2}{4} + 0.236\mu} \quad (14)$$

Shown in Figure 4-4, are three curves for (G_{eff}/E) vs. a for the case where the fundamental vibration frequency of 10 Hz has been used to eliminate μ . The three curves correspond to three different values for (r_g/ℓ). It is shown in the figure that for all cases of practical interest, the minimum required G_{eff} need be at most two or three orders of magnitude smaller than E .

4.1.6 Comments on Lattice Beam

Since the parametric studies indicate that the best cylindrical beam design is that with a very large radius and a minimum wall thickness, it is expected that further reduction of weight may be achieved with a lattice beam configuration. It is likely that such a design will result in significant weight savings, but may also result in increased beam radius. The blocked area ratio is also likely to be reduced. However, the complex pattern of shadows created by a lattice beam may tend to diminish somewhat the gains in blocked area.

4.2 RIM-TRIPOD CONFIGURATION

An alternate concept for the FSS is that of a tripod in which the three equally spaced legs are cantilevered at the feed device and pinned at the reflector rim. A schematic of this configuration is shown in Figure 4-5.

For this configuration, it is assumed that the structural behavior of the tripod is essentially that of a truss for vertical motion. For pure rotation of the feed device about any axis, the tripod legs are assumed to provide resistance by bending. Furthermore, the local vibration of each leg is assumed to be governed in bending in the simply supported mode.

4.2.1 Fundamental Frequency of Vibration of Individual Struts

It is assumed that each leg or strut of the tripod has a natural frequency of vibration which is governed by bending in the simply supported mode. The well-known result for the lowest frequency in this case is

$$f_n = \frac{1}{2\pi} \left(\frac{\pi^2}{\ell^2} \right) \sqrt{\frac{EI}{\rho A}} \quad (15)$$

where

$$\begin{aligned} E &= \text{Modulus of elasticity of strut material} \\ \rho &= \text{Mass density of strut material} \\ \ell &= \text{Length of strut} \\ I &= \text{Moment of inertia of strut cross-section} \\ A &= \text{Area of strut cross-section} \end{aligned} \quad (16)$$

As shown in Figure 4-6, the geometry of the configuration requires the strut length ℓ to be

$$\ell = \sqrt{(7.5m)^2 + (9.25m)^2} = 11.9m \quad (17)$$

Assuming that each strut is a thin-walled tube of radius r and wall thickness t , the moment of inertia I and area A of each strut may be expressed as

$$\begin{aligned} I &\equiv \pi r^3 t \\ A &\equiv 2\pi r t \end{aligned} \quad (18)$$

Substituting from equation (18) into equation (15), it can be shown that

$$f_n = \frac{1}{2\pi} \left(\frac{\pi^2}{\ell^2} \right) \frac{r^2}{\sqrt{2}} \sqrt{\frac{E}{\rho}} \quad (19)$$

Note that the fundamental strut frequency is independent of wall thickness for a thin-walled tube.

Using the numerical values of $E = 22.7 \times 10^9 \text{ N/m}^2$, $\rho = 1,740 \text{ kg/m}^3$, and $\ell = 11.9 \text{ m}$, equation (19) results in

$$f_n = (89.7 \text{ Hz/m}) r \quad (20)$$

4.2.2 Fundamental Frequency of Vibration for Rotation of Feed Device About Any Strut Axis

The entire tripod-feed device system has several overall modes of vibration. One mode of particular concern for the tripod configuration considered here is that of pure rotation of the feed device. Such motion cannot be resisted by truss action in this case and depends instead on a moment-carrying connection of the struts at the feed device.

A mode of rotational vibration which is likely to provide a good estimate of the lowest rotational frequency is that of pure feed rotation about a strut axis. Such a mode will produce no strain energy in one of the struts, and will induce bending strain energy in the other two. This assumes that the torsional stiffness of the strut in pure torsion is negligible due to (1) low effective shear modulus of the composite tube strut, and (2) low torsional restraint provided by the pinned connection at the reflector rim.

Consider a planar view of the FSS, where the plane of interest is defined by the intersecting centerlines of two struts AB and AC, as shown in Figure 4-7. For the rim-tripod geometry, the angle α may be computed as

$$\alpha = \cos^{-1} \left[\frac{(10\mathbf{i} + 8.12\mathbf{k}) \cdot (-5\mathbf{i} - 8.66\mathbf{j} + 8.12\mathbf{k})}{12.882 \cdot 12.882} \right] = 84.49^\circ \quad (21)$$

Now, for a rotation of the feed through an angle θ about the axis of strut AB, the induced tip deflection Δ in cantilevered strut AC may be expressed as

$$\Delta \equiv (10m) \theta \cos\left(\alpha - \frac{\pi}{2}\right) = (9.954m) \theta \quad (22)$$

The shear force in strut AC at C (or the tip load in the cantilever) may be computed as

$$P = \frac{3EI\Delta}{\ell^3} = \frac{3EI}{\ell^3} (9.954m) \theta \quad (23)$$

Since the strut not shown in Figure 4-7 must undergo an identical deflection Δ with an identical tip load P , the restoring moment about the AB strut axis due to bending in the other two struts may be written as

$$\text{Moment} = 2P(9.954m) = 2\left(\frac{3EI}{\ell^3}\right) (9.954m)^2 \theta \quad (24)$$

The torsional stiffness for this rotational motion may be obtained by dividing the restoring moment from equation (24) by the angle of rotation θ to obtain

$$k_{\theta} = \frac{6EI(9.954m)^2}{\ell^3} \quad (25)$$

where E , I , and ℓ are as defined in equation (16).

The fundamental frequency of vibration for this rotational motion may be written as

$$f_n = \frac{1}{2\pi} \sqrt{\frac{k_{\theta}}{I_p}} \quad (26)$$

where k_{θ} is the torsional stiffness given by equation (25), and

$$I_p = M_{\text{feed}} r_g^2 \quad \text{Mass moment of inertia of feed device} \quad (27)$$

Where M_{feed} is the mass of the feed device, and r_g is the radius of gyration of the feed device, as previously defined.

Substituting from equations (18), (25), and (27) into (26) it can be shown that

$$f_n = \frac{1}{2\pi} (9.954m) \sqrt{\frac{6E\pi}{M_{\text{feed}} r_g^2 \ell^3}} \cdot \sqrt{r^3 t} \quad (28)$$

Using the numerical values of $E = 227.5 \times 10^9 \text{ N/m}^2$, $M_{\text{feed}} = 300 \text{ kg}$, $r_g = 0.5 \text{ m}$, and $\ell = 12.9 \text{ m}$ (effective strut length to the center of the feed device), equation (28) results in

$$f_n = (8180 \text{ Hz/m}^2) \sqrt{r^3 t} \quad (29)$$

4.2.3 Fundamental Frequency of Vibration for Vertical Translation of Feed Device

Another of the overall modes of vibration of the FSS is that of simple vertical translation of the feed device without rotation.

Referring to the diagram in Figure 4-6, the change in length δ of each strut resulting from a vertical displacement Δ of the feed device may be written as

$$\delta = \Delta \sin(39.07^\circ) \quad (30)$$

The axial force F thereby induced by stretching in each strut may be written as

$$F = \left(\frac{EA}{\ell}\right)\delta = \frac{EA\Delta}{\ell} \sin(39.07^\circ) \quad (31)$$

The vertical component F_v of each strut force may be written as

$$F_v = F \sin(39.07^\circ) = \frac{EA\Delta}{\ell} [\sin(39.07^\circ)]^2 \quad (32)$$

Thus, the total vertical restoring force $3F_v$ in the three struts may be divided by the vertical deflection Δ in order to provide the stiffness k_v for vertical translation

$$k_v = \frac{3F_v}{\Delta} = \frac{3EA}{\ell} [\sin(39.07^\circ)]^2 \quad (33)$$

The natural frequency of vibration for vertical translation may then be estimated as

$$f_n = \frac{1}{2\pi} \sqrt{\frac{k_v}{M_{\text{feed}}}} \quad (34)$$

Substituting from equations (18) and (33) into equation (34), it can be shown that

$$f_n = \frac{1}{2\pi} \sqrt{\frac{6\pi E r t}{M_{\text{feed}} \ell}} \sin(39.07^\circ) \quad (35)$$

Using the numerical values $E = 227.5 \times 10^9 \text{ N/m}^2$, $M_{\text{feed}} = 300 \text{ kg}$, and $\ell = 11.9 \text{ m}$, it can be shown that

$$f_n = (3480 \text{ Hz/m}^2) r t \quad (36)$$

4.2.4 Blocked Area Ratio

For the rim-tripod configuration, the blocked or shaded area due to the three struts is

$$A_{\text{block}} = 3(2r)(9.25m) = (55.5m) r \quad (37)$$

where r is the radius of a strut. From equation (5), the total front area of the reflector is

$$A_{\text{frontal}} = \pi(10m)^2 = 314.2m^2$$

Thus, the blocked area ratio a in this case is

$$a = \frac{A_{\text{block}}}{A_{\text{frontal}}} = (0.177/m) r \quad (38)$$

Equivalently, the strut radius r may be expressed in terms of the blocked area ratio a as

$$r = (5.66m) a \quad (39)$$

4.2.5 Structural Mass Ratio

As defined in equation (9), the structural mass ratio μ is

$$\mu = \frac{M_{\text{FSS}}}{M_{\text{feed}}} = \frac{M_{\text{FSS}}}{300kg}$$

In the rim-tripod configuration, the mass M_{FSS} of the FSS is simply the mass of the three struts, which may be written as

$$M_{\text{FSS}} = 3\rho A\ell \quad (40)$$

Substituting from equations (18) and (40) into (9), it can be shown that

$$\mu = \frac{3\rho(2\pi r t)\ell}{300kg} \quad (41)$$

Using the numerical values $\rho = 1740 \text{ kg/m}^3$ and $\ell = 11.9m$ in equation (41) yields

$$\mu = (1301/m^2) r t \quad (42)$$

Equivalently, the product rt may be expressed in terms of the structural mass ratio μ as

$$rt = (7.69 \times 10m^2) \mu \quad (43)$$

4.2.6 Parametric Studies

By substituting from equations (39) and (43) into equations (20), (29), and (36), the various natural frequencies may be expressed directly in terms of the blocked area ratio a and structural mass ratio μ . The resulting parametric equations are

$$f_n = (507\text{Hz}) a \quad \text{Strut frequency} \quad (44)$$

$$f_n = (1280\text{Hz}) a \mu^{\frac{1}{2}} \quad \text{Pure rotation frequency} \quad (45)$$

$$f_n = (96.5\text{Hz}) a \mu^{\frac{1}{2}} \quad \text{Vertical translation frequency} \quad (46)$$

To clearly illustrate these relations, curves of μ vs. a are sought, with system lowest natural frequency f_n treated as a parameter. To this end, equations (44), (45) (46) may be re-written as

$$\begin{aligned} a &\geq \left(\frac{f_n}{507\text{Hz}} \right) && \text{Strut frequency} \\ \mu &\geq \left(\frac{f_n}{1280\text{Hz}} \right)^2 \frac{1}{a^2} && \text{Pure rotation frequency limit} \\ \mu &\geq \left(\frac{f_n}{96.5\text{Hz}} \right)^2 && \text{Vertical translation frequency} \end{aligned} \quad (47)$$

All three requirements of equations (47) must apply simultaneously, with one or another actually governing in different regions in the μ, a plane.

Shown in Figure 4-8 are three curves corresponding to system natural frequencies of $f_n = 5\text{Hz}$, 10Hz and 20Hz , respectively. It is seen that the curves generally fall from upper left to lower right. Starting from upper left, each curve begins with a vertical segment, corresponding to a cut-off value of blocked area ratio a determined by the local strut resonance. Next, for $f_n = 5\text{Hz}$ or 10Hz , there is a steeply curved segment determined by the pure rotation frequency of the system. Finally, each curve ends with a horizontal segment determined by the vertical translation frequency of the system.

Also shown in Figure 4-8 are several contours for the design parameters r and t , obtained from equations (39) and (43). These contours may be used together with the parametric curves just described, to gain a complete description of the design corresponding to any location in the μ, α plane, and its general operating characteristics. For example, the best design corresponding to a lowest overall natural frequency of 10 Hz, and consistent with a minimum strut wall thickness of 1 mm, has a strut radius of about 11.5 cm. For this design, the lowest natural frequency of 10 Hz occurs in the pure rotation mode, and the blocked area ratio is about 2 percent. Furthermore, the structural mass ratio is about 15 percent. Note that these numbers are much more favorable than those obtained for the previous case of a cantilever configuration.

4.3 SUNSHADE-TRIPOD CONFIGURATION

Another closely related concept for the FSS is that of another tripod in which the three equally spaced legs are again cantilevered at the feed device, but in this case the other ends of the legs are pinned at a certain location on the sunshade. A schematic of this configuration is shown in Figure 4-9.

In this configuration, use is made of the truss structure supporting the sunshade in order to attach the feed support structure. Note that the configuration is nearly identical to that of the rim-support structure, except that the legs are significantly shorter, and the least angle between the reflector axis and any leg is significantly larger. The structural behavior for this configuration is assumed to be identical to that of the rim-tripod configuration.

4.3.1 Fundamental Frequency of Vibration of Individual Struts

As shown in Figure 4-10, it is assumed in this case that the least angle β between the reflector axis and any leg of the tripod is 75 degrees (studies of the case where $\beta = 80$ degrees revealed that the vertical translation frequency was unacceptably low).

For the geometry shown in Figure 4-10, the strut length l in this case is

$$l = \frac{9.25m}{\cos 15^\circ} = 9.58m \quad (48)$$

Substituting for ℓ from equation (48), and using the numerical values $E = 227.5 \times 10^9 \text{ N/m}^2$ and $\rho = 1740 \text{ kg/m}^3$ in equation (19), one obtains

$$f_n = (138 \text{ Hz/m}) r \quad (49)$$

for the fundamental frequency of vibration of an individual strut.

4.3.2 Fundamental Frequency of Vibration for Rotation of Feed Device About Any Strut Axis

The sunshade-tripod configuration will have a natural mode of vibration dominated by pure rotational motion of the feed device, similar to that described in Section 4.2 for the rim-tripod configuration.

Referring to Figure 4-7 for the geometry of the sunshade-tripod configuration, it can be shown that

$$\alpha = \cos^{-1} \left[\left(\frac{10 \mathbf{i} + 2.68 \mathbf{k}}{10.35} \right) \cdot \left(\frac{-5 \mathbf{i} - 8.66 \mathbf{j} + 2.68 \mathbf{k}}{10.35} \right) \right] = 113.6^\circ \quad (50)$$

Substituting from equation (50) for α , and setting $\ell = 10.35 \text{ m}$ (effective strut length to center of feed device), following the analysis of Section 4.2 leads to

$$f_n = (10,500 \text{ Hz} / \text{m}^2) \sqrt{r^3 t} \quad (51)$$

This represents an estimate of the fundamental frequency of vibration of the sunshade-tripod configuration in the pure feed rotation mode, as described in Section 3.2.

4.3.3 Fundamental Frequency of Vibration for Vertical Translation of Feed Device

Following the analysis of Section 4.2, the fundamental frequency of vibration for vertical translation in the case of the sunshade-tripod configuration may be estimated in a similar manner. However, due to the different geometry shown in Figure 4-10, the change in length δ of each strut resulting from a vertical displacement Δ of the feed device may be written as

$$\delta = \Delta \sin(15^\circ) \quad (52)$$

Following the previous analysis, it may be shown in this case that the fundamental frequency f_n is

$$f_n = \frac{1}{2\pi} \sqrt{\frac{6\pi E r t}{M_{feed} \ell}} \sin(15^\circ) \quad (53)$$

where all variables are as identified in Section 4.2.

Substituting from equation (48) for ℓ , and using the numerical values $E = 227.5 \times 10^9 \text{ N/m}^2$, and $M_{feed} = 300 \text{ kg}$, equation (53) results in the relation

$$f_n = (1590 \text{ Hz} / \text{m}) \sqrt{r t} \quad (54)$$

4.3.4 Blocked Area Ratio

Comparing sunshade-tripod configuration and the rim-tripod configuration, it is clear that the blocked area, and hence the blocked area ratio a for each configuration is defined identically. Thus, a and the strut radius r are related by equations (38) and (39), as presented in Section 4.2.4.

4.3.5 Structural Mass Ratio

Substituting from equations (48) for ℓ , into equation (41) of Section 4.2.6, and using the numerical value $\rho = 1740 \text{ kg/m}^3$, it can be shown that

$$\mu = (1047 / \text{m}^2) r t \quad (55)$$

Equivalently, the product $r t$ may be expressed in terms of the structural mass ratio μ as

$$r t = (9.55 \times 10^{-4} \text{ m}^2) \mu \quad (56)$$

4.3.6 Parametric Studies

By substituting from equations (39) and (56) into equations (49), (51) and 54), the various natural frequencies may be expressed directly in terms of the blocked area ratio a and structural mass ratio μ . The resulting parametric equations are

$$f_n = (781 \text{ Hz})a \dots \text{Strut frequency} \quad (57)$$

$$f_n = (1840 \text{ Hz})a\mu \dots \text{Pure rotation frequency} \quad (58)$$

$$f_n = (49.1 \text{ Hz})\mu^{\frac{1}{2}} \dots \text{Vertical translation frequency} \quad (59)$$

Rewriting equations (57), (58) and (59) in the form of μ vs. a with a system lowest nature frequency f_n treated as a parameter, one finds

$$\begin{aligned} a &\geq \left(\frac{f_n}{781 \text{ Hz}} \right) && \text{Strut frequency limit} \\ \mu &\geq \left(\frac{f_n}{1840 \text{ Hz}} \right)^2 \frac{1}{a^2} && \text{Pure rotation frequency limit} \\ \mu &\geq \left(\frac{f_n}{49.1 \text{ Hz}} \right)^2 && \text{Vertical translation frequency limit} \end{aligned} \quad (60)$$

All three requirements of equations (60) must apply simultaneously, with one or another actually governing in different regions in the μ , a plane.

Shown in Figure 4-11 are three curves corresponding to system natural frequencies of $f_n = 5 \text{ Hz}$, 10 Hz and 20 Hz , respectively. All of the same general trends apply to the curves in Figure 4-11 as those of the rim-tripod configuration in Figure 4-8.

Comparing the Figures 4-8 and 4-11 for $f_n = 10 \text{ Hz}$ designs with a minimum wall thickness of $t = 1 \text{ mm}$, one finds that the required strut radius for the sunshade-tripod configuration is about 9.5 cm (see Figure 4-11). For this design, the lowest natural frequency of 10 Hz occurs in the pure rotation mode, as in the case of the rim-tripod configuration. Furthermore, the blocked area ratio for the sunshade-tripod design is about 1.7 percent, and the structural mass ratio is about 10.5 percent. It is noteworthy that these results are significantly more favorable than those obtained from the rim-tripod configuration.

4.4 RADIAL SPOKE BICYCLE WHEEL CONFIGURATION

A well-proven concept for very lightweight structures is that of pretensioned cable-stayed configurations. By utilizing the high structural efficiency of materials loaded

only in uniaxial tension, truss-like structural behavior may be obtained from cable nets, when properly pretensioned.

Many pretensioned cable configurations are possible. Two particular examples are considered in this report. First, a radial spoke bicycle wheel configuration is considered in this section, and then an interlaced spoke bicycle wheel configuration is considered in the next section.

Shown in Figure 4-12, is the radial spoke bicycle wheel (RSBW) configuration. In this configuration, the feed device, which is assumed to be cylindrical in shape with the dimensions shown, is supported by twelve equally spaced pairs of radial wires, or spokes, as shown. Each pair of wires consists of an upper wire and a lower wire. They attach to the upper and lower circular perimeter of the feed device, respectively, and attach to a common anchor point in a reinforced ring structure within the sunshade support truss. The anchor points for all twelve pairs of wires lie on a circle whose center is coincident with the center of the cylindrical feed device.

The radial wires are pretensioned to provide structural stiffness. The structural behavior of the RSBW FSS will involve truss-like behavior of the wires for nearly all important feed motions.

The vibration modes of the RSBW will include low frequencies associated with (1) individual wire resonance, (2) vertical feed translation, (3) rocking of the feed about an axis normal to the reflector axis, and (4) rotation (or torsion) of the feed about the reflector axis. The design of the RSBW FSS, which consists of selecting the radius of the wires and their pretension, is based herein on concern for the fundamental frequency of vibration of the system.

4.4.1 Required Wire Tensile Stress

The pretension in the wires must be adequate to provide a local wire resonant frequency which is higher than the fundamental frequency of the complete RSBW FSS system. It is well known that the fundamental frequency of vibration of a string is given by

$$f_w = \frac{1}{2\ell} \sqrt{\frac{T}{\rho A}} = \frac{1}{2\ell} \sqrt{\frac{\sigma_0}{\rho}} \quad (61)$$

where T is the tension force in the string, ρ is the mass density of the string material, σ_0 is the tensile stress in the string, and ℓ is the length of the string.

If the fundamental frequency of the wire is selected, then the required tensile stress σ_0 may be determined as

$$\sigma_0 = 4\ell^2 f_w^2 \rho \quad (62)$$

Using the values of $\rho = 1740 \text{ kg/m}^3$, and (from the geometry shown in Figure 4-12)

$$\ell = \sqrt{(9.25\text{m})^2 + (0.75\text{m})^2} = 9.28\text{m} \quad (63)$$

equation (62) then requires

$$\sigma_0 \begin{cases} 59.9 \text{ MN} / \text{m}^2 \text{ for } f_w = 10 \text{ Hz} \\ 240 \text{ MN} / \text{m}^2 \text{ for } f_w = 20 \text{ Hz} \end{cases} \quad (64)$$

The minimum weight structure will result from using the material in an optimally stressed manner. Thus, an estimate of the maximum allowable stress in the material is important.

Assuming linear material behavior and a maximum allowable strain of about 1.05×10^{-3} results in a value of maximum working stress σ_{\max} of

$$\sigma_{\max} = E\epsilon_{\max} = (227.5 \times 10^9 \text{ N} / \text{m}^2)(1.05 \times 10^{-3}) = 228 \text{ MN} / \text{m}^2 \quad (65)$$

This value is within about 5 percent of the stress required for a 20 Hz wire frequency. Thus, the design will henceforth be based on an assumption that $\sigma_2 = 240 \text{ MN/m}^2$. This will result in a local wire fundamental frequency of 20 Hz, and also will result in a minimum weight structure.

4.4.2 Fundamental Frequency of Vibration for Vertical Translation of Feed Device

Referring to the geometry of Figure 4-12, the change in length δ of each wire resulting from a vertical displacement Δ of the feed device may be written as

$$\delta = \Delta \sin \theta$$

$$\theta = \tan^{-1}\left(\frac{0.75}{9.25}\right) = 4.64^\circ \quad (66)$$

As a result, the change in tension ΔT in each wire is

$$\Delta F = \frac{EA\delta}{\ell} = \frac{EA\Delta}{\ell} \sin \theta \quad (67)$$

where A is the cross-sectional area of any wire, and ℓ is the length of a wire, as given by equation (63). The net vertical restoring force F from 24 identical wires is

$$F = 24\Delta F \sin \theta = \frac{24EA}{\ell} \sin^2 \theta \Delta \quad (68)$$

Thus, the effective vertical stiffness of the FSS is

$$k_v = \frac{F}{\Delta} = \frac{24EA}{\ell} \sin^2 \theta \quad (69)$$

The fundamental frequency of vertical vibration of the feed device may now be estimated as

$$f_n = \frac{1}{2\pi} \sqrt{\frac{k_v}{M_{\text{feed}}}} = \frac{1}{2\pi} \sqrt{\frac{24EA \sin^2 \theta}{\ell M_{\text{feed}}}} \quad (70)$$

If the radius of any wire is r , A may be expressed as

$$A = \pi r^2 \quad (71)$$

Substituting equation (71) into equation (70), one finds

$$f_n \left(\frac{1}{2\pi} \sqrt{\frac{24\pi E}{\ell M_{\text{feed}}}} \sin \theta \right) r \quad (72)$$

Using the numerical values $E = 227.5 \times 10^9 \text{ N/m}^2$, $M_{\text{feed}} = 300 \text{ kg}$, ℓ from equation (63), and θ from equation (66), it can be shown that

$$f_n = (1,010 \text{ Hz} / m) r \quad (73)$$

4.4.3 Fundamental Frequency of Vibration for Pure Rocking of the Feed About an Axis Normal to the Reflector Axis

One mode of vibration of concern is that of pure rotation of the feed mass about any axis perpendicular to the reflector axis. As a special case, analysis is presented for a rotational axis which is the bisector of a single pair of upper and lower wires. For rotation about this axis through an angle θ , 20 of the 24 wires will experience changes in length, causing unbalanced forces, which in turn produce a restoring moment.

To analyze this situation, consider the geometry shown in Figure 4-13, which defines the z-axis as the axis of rotation, and numbers the wire attachment points around the perimeter of the feed device. In Figure 4-14, the solid lines represent the undeformed feed position, and the dashed lines represent the rotated position. During the motion, attachment point B moves to point B', so that wire AB moves to position AB'.

For any wire AB, let \underline{p} be a vector from A to B, thereby denoting the original position of the wire. Since the original length of all wires is ℓ (where ℓ is given by equation (63), \underline{p} may be expressed as

$$\underline{p} = \ell \underline{e} \quad (74)$$

where \underline{e} is a unit vector directed from A to B. Now let \underline{u} be the displacement vector of point B, going from B to B'. Then the vector \underline{p}' which denotes the position AB' in the rotated configuration may be expressed as

$$\underline{p}' = \underline{p} + \underline{u} = \ell \underline{e} + \underline{u} \quad (75)$$

The length of ℓ' of wire AB' in the deformed configuration may be expressed as

$$\ell' = (\underline{p}' \cdot \underline{p}')^{\frac{1}{2}} = [(\ell \underline{e} + \underline{u}) \cdot (\ell \underline{e} + \underline{u})]^{\frac{1}{2}} = (\ell^2 + 2\ell \underline{e} \cdot \underline{u} + \underline{u} \cdot \underline{u})^{\frac{1}{2}} \quad (76)$$

For small rotations $\underline{u} \ll \ell$ so that the last term in equation (76) may be discarded, and the binomial theorem may be used to estimate ℓ' as

$$\ell' \cong \ell + \underline{e} \cdot \underline{u} \quad (77)$$

Hence, the change in length δ of the wire is

$$\delta = \ell' - \ell = \underline{\mathbf{e}} \cdot \underline{\mathbf{u}} \quad (78)$$

The resulting change in wire tension ΔT is

$$\Delta T = \frac{EA}{\ell} \delta = \frac{EA}{\ell} (\underline{\mathbf{e}} \cdot \underline{\mathbf{u}}) \quad (79)$$

Assuming the rotation is sufficiently small that changes in the direction of wire tension forces may be neglected, then the unbalanced force $\underline{\mathbf{F}}$ on the feed device from one wire is

$$\underline{\mathbf{F}} = -\Delta T \underline{\mathbf{e}} = -\frac{EA}{\ell} (\underline{\mathbf{e}} \cdot \underline{\mathbf{u}}) \underline{\mathbf{e}} \quad (80)$$

The restoring moment resulting from this rotation may then be determined by summing the moments about the axis of rotation produced by each restoring force $\underline{\mathbf{F}}$.

The x , y , z components of $\underline{\mathbf{e}}$ and $\underline{\mathbf{u}}$ for each attachment point shown in Figure 4-13 are presented in Table 4-1, together with the scalar quantities δ , ΔT , and the corresponding restoring moment about the z -axis (e.g., axis of rotation).

From the results in Table 4-1 and the geometry in Figure 4-13, the total restoring moment caused by changes in tension in all spokes is

$$\mathbf{M} = \left[8(0.4041 \text{ m})^2 + 8(0.6999 \text{ m})^2 + 4(0.8081 \text{ m})^2 \right] \frac{EA}{\ell} \theta = (7.84 \text{ m}^2) \frac{EA}{\ell} \theta \quad (81)$$

Hence, the torsional stiffness for this mode of rocking vibration is

$$\mathbf{k}_\theta = \frac{\mathbf{M}}{\theta} = (7.84 \text{ m}^2) \frac{EA}{\ell} \quad (82)$$

Therefore, the natural frequency for this mode is given by

$$f_n = \frac{1}{2\pi} \sqrt{\frac{\mathbf{k}_\theta}{I_p}} \cong \frac{1}{2\pi} \sqrt{\frac{(7.84 \text{ m}^2) EA}{\ell M_{\text{feed}} r_g^2}} \quad (83)$$

Substituting from equation (71) for \mathbf{A} in terms of r , equation (83) may be rewritten as

$$f_n = \frac{1}{2\pi} \sqrt{\frac{(7.84m^2)\pi E}{\ell M_{\text{feed}} r_g^2} r} \quad (84)$$

Using the numerical values $E = 227.5 \times 10^9 \text{ N/m}^2$, $M_{\text{feed}} = 300 \text{ kg}$, $r_g = 0.5 \text{ m}$, and $\ell = 9.28 \text{ m}$ (from equation (63)), equation (84) yields

$$f_n = (14,300 \text{ Hz/m})r \quad (85)$$

4.4.4 Fundamental Frequency of Vibration for Pure Torsion of the Feed about the Reflector Axis

Of primary concern for this radial spoke bicycle wheel configuration is the fundamental frequency of vibration for pure torsional motion about the reflector axis. This is because the radial spoke configuration is capable of rotating about the reflector axis without appreciable change in tension of the spokes. Thus, the restoring moment is small, and the stiffness is provided solely by geometric effects.

Assuming the tension in each spoke remains constant for this type of small rotation of angle θ about the reflector axis, the total restoring moment from all 24 spokes may be written as

$$M = 24 \frac{(0.75m)\theta}{\ell} (0.75m)T_0 \quad (86)$$

where σ_0 is the initial tension in the spokes, which is given by

$$T_0 = \sigma_0 \pi r^2 \quad (87)$$

where $\sigma_0 = 240 \text{ MN/m}^2$ is the prestress in the spokes.

The torsional stiffness k_T is therefore

$$k_T = \frac{M}{\theta} = 24 \frac{(0.75m)^2}{\ell} \sigma_0 \pi r^2 \quad (88)$$

The fundamental frequency of torsional vibration may therefore be expressed as

$$f_n = \frac{1}{2\pi} \sqrt{\frac{k_T}{I_p}} = \frac{1}{2\pi} \sqrt{\frac{24(0.75m)^2 \sigma_0 \pi r^2}{\ell M_{feed} r_g^2}} \quad (89)$$

Using the numerical values $\sigma_0 = 240 \text{ MN/m}^2$, M_{feed} , $r_g = 0.5 \text{ m}$, and $\ell = 9.28 \text{ m}$ (from equation (63)), it can be shown that

$$f_n = (609 \text{ Hz} / m)r \quad (90)$$

4.4.5 Blocked Area Ratio

The frontal area blocked by a single spoke is

$$A_{spoke} = 2r(9.25m) \quad (91)$$

Where r is the radius of a spoke. Since the spokes are arranged in pairs which lie in planes passing through the reflector axis, one spoke lies directly beneath the other in each pair, as shown in Figure 4-12. Thus, the total blocked area may be calculated as 12 A_{spoke} . However, slight fabrication errors are likely to result in substantial increase in the blocked area ratio. In order to account for this effect, we instead use the worst case value

$$\begin{aligned} A_{blocked} &= 24A_{spoke} = 48r(9.25m) \\ A_{blocked} &= (444m)r \end{aligned} \quad (92)$$

which results when no spoke is shadowed by another.

The blocked area ratio a is then

$$a = \frac{A_{blocked}}{\pi(10m)^2} = (1.41m)r \quad (93)$$

Or, equivalently

$$r = (0.708m)a \quad (94)$$

4.4.6 Structural Mass Ratio

The mass M_{FSS} of the feed support structure for this RSBW configuration is

$$M_{FSS} = 24\rho A\ell = 24\pi r^2\rho\ell \quad (95)$$

Using the numerical values $\rho = 1740 \text{ kg/m}^3$, and $\ell = 9.28 \text{ m}$ from equation (63), it can be shown that

$$M_{FSS}(1.22 \times 10^6 \text{ kg} / \text{m}^2)r^2 \quad (96)$$

Dividing M_{FSS} by the feed mass M_{feed} yields the structural mass ratio μ where

$$\mu = \frac{M_{FSS}}{M_{feed}} = \frac{(1.22 \times 10^6 \text{ kg} / \text{m}^2)r^2}{(300\text{kg})} = (4,070 \text{ m}^2)r^2 \quad (97)$$

4.4.7 Parametric Studies

By substituting from equation (94) into equations (73), (85) and (90), the various natural frequencies may be expressed directly in terms of the blocked area ratio a . The resulting parametric equations are

$$f_n = (715 \text{ Hz})a \dots \text{Vertical translation frequency} \quad (98)$$

$$f_n = (10,100 \text{ Hz})a \dots \text{Rocking frequency} \quad (99)$$

$$f_n = (431 \text{ Hz})a \dots \text{Torsional frequency} \quad (100)$$

Note that in each case the natural frequencies may be expressed either in terms of a or μ . That is, a and μ are related through equations (94) and (97) as

$$\mu = 2040 a^2 \quad (101)$$

It is clear from equations (98), (99) and (100) that all RSBW configurations are governed by the torsional frequency requirement.

Shown in Figure 4-15 are three curves which represent the dependence of the fundamental frequency for rocking, vertical translation and torsion (respectively) as functions of the blocked area ratio a . Shown along the bottom edge of the figure is an alternative scale in terms of the structural mass ratio μ . All of the curves in the figure are based on the assumption that the initial stress in the spokes is 240 MPa so that the corresponding local string frequency of each spoke is 20 Hz . Also shown in the figure are vertical lines corresponding to contours of values for constant spoke radius, r .

From the governing curve for torsional frequency in Figure 4-15, an RSBW with a fundamental frequency of 10 Hz is seen to have a worst-case blocked area ratio of about 2.3 percent, and a corresponding structural mass ratio of about 120 percent. These numbers would not appear to be attractive in comparison with, for example, the sunshade-tripod design described in the previous section. This is particularly true when one notes that the required spoke radius of about 17 cm and initial stress of 240 MN/m^2 requires an initial tension force in each spoke of $21,800 \text{ kN}$. Such large tension loads could not be supported by the sunshade structure without substantial modification and added weight. Since the particular bicycle wheel configuration studied in this section does not appear to be competitive, no attempt was made to account for this added rim mass. However, a more competitive version of the bicycle wheel is considered in the next section, where the analysis for required additions to the rim are presented.

4.5 INTERLACED SPOKE BICYCLE WHEEL CONFIGURATION

The radial spoke bicycle wheel configuration analyzed in the previous section was found to be governed by a relatively low stiffness for torsional motion about the reflector axis. This inherent low stiffness was due to the lack of truss action in resisting torsional motion, and resulted in excessive structural mass and preloading in the rim.

Shown in Figure 4-16 is the interlaced spoke bicycle wheel (ISBW) configuration. Comparing Figure 4-12 and 4-16, it is apparent that the ISBW and RSBW configurations are identical except for the rigging of the twelve pairs of spokes. In the ISBW configuration, each pair of spokes attached at a common rim supported point and alternately at upper and lower feed attachment points which are diametrically opposed. In this configuration, even the torsional mode of vibration about the reflector axis is resisted by truss action of the spokes.

4.5.1 Required Spoke Tensile Stress

In the ISBW configuration, an analysis similar to that presented in Section 4.1, shows that the required tensile stress σ_0 is again given by equation (62) where, in this case

$$l = \sqrt{(10m)^2 + (0.75m)^2 + (0.75m)^2} = 10.06m \quad (102)$$

as seen from the geometry in Figure 4-16.

Substituting from equation (102) into equation (62), and using the numerical value: $\rho = 1740 \text{ kg/m}^3$, it can be shown that

$$\sigma_0 = \begin{cases} 70.4MN / m^2 & \text{for } f_s = 10\text{Hz} \\ 282MN / m^2 & \text{for } f_s = 20\text{Hz} \end{cases} \quad (103)$$

Assuming a local string frequency of $f_s = 20 \text{ Hz}$, and a modulus of elasticity of $227.5 \times 10^9 \text{ N/m}^2$, the required stress given in equation (103) results in a working strain of

$$\epsilon = \frac{\sigma_0}{E} = \frac{282 \times 10^6 \text{ N/m}^2}{227.5 \times 10^9 \text{ N/m}^2} = 0.124\% \quad (104)$$

4.5.2 Fundamental Frequency of Vibration for Vertical Translation of Feed Device

Following a procedure similar to that given in Section 4.4.2, the vertical stiffness of the ISBW configuration can be shown to be

$$k_v = 24 \frac{EA}{\ell} (7.46 \times 10^{-2})^2 \quad (105)$$

Hence, the fundamental frequency of vertical vibration of the feed device may be estimated as

$$f_n = \frac{1}{2\pi} \sqrt{\frac{k_v}{M_{\text{feed}}}} = \frac{1}{2\pi} \sqrt{\frac{24EA(7.4610^{-2})^2}{\ell M_{\text{feed}}}} \quad (106)$$

Substituting for **A** in terms of the spoke radius **r** from equation (71), equation (106) leads to

$$f_n = \left(\frac{1}{2\pi} \sqrt{\frac{24\pi E}{\ell M_{\text{feed}}} (7.47 \times 10^{-2})} \right) r \quad (107)$$

Using the numerical values $E = 227.5 \times 10^9 \text{ N/m}^2$, $M_{\text{feed}} = 300 \text{ kg}$, and ℓ from equation (102), it can be shown that

$$f_n = (896 \text{ Hz/m}) r \quad (108)$$

4.5.3 Fundamental Frequency of Vibration for Pure Rocking of the Feed About an Axis Normal to the Reflector Axis

As shown for the RSBW configuration in Section 4.4.3, the vibration mode of pure rocking of the feed about an axis normal to the reflector axis results in a large change in strain energy in the spokes, and consequently a high frequency of vibration. As shown in Figure 4-15, the fundamental frequency of vibration for this mode is much higher than either the vertical translation or torsional modes for the RSBW configuration.

While the ISBW configuration is different from the RSBW configuration, the differences do not appreciably change the behavior for rocking vibration. Thus, it is again expected that the rocking vibration frequency will be far higher than either the vertical

translation or torsion frequencies, and thus it will not be an important consideration in design.

4.5.4 Fundamental Frequency of Vibration for Pure Torsion of the Feed About the Reflector Axis

Unlike the RSBW configuration, torsional motion of the feed device in the ISBW configuration is resisted by truss action of the spokes. To determine the torsional stiffness of the ISBW configuration, consider the geometry of deformation of a single spoke AB, as shown in Figure 4-17.

As the feed device rotates through an angle θ as shown, point B moves to point B'. The resulting displacement vector of point B is

$$\underline{u} = -(0.75 \text{ m}) \theta \mathbf{i} \quad (109)$$

The resulting elongation of spoke AB is given by

$$\Delta \ell = (0.75 \text{ m}) \theta \left(\frac{10 \text{ m}}{10.06 \text{ m}} \right) = (0.746 \text{ m}) \theta \quad (110)$$

As a result of the change in length of the spoke, the tension force in the spoke changes an amount ΔF where

$$\Delta F = \frac{EA}{\ell} \Delta \ell = \frac{EA}{\ell} (0.746 \text{ m}) \theta \quad (111)$$

The restoring moment produced by the change in tension in the spoke is

$$\Delta M_{\text{res}} = \Delta F \left(\frac{10 \text{ m}}{10.06 \text{ m}} \right) (0.746 \text{ m}) \theta \quad (112)$$

Thus, the restoring moment due to 24 spokes of essentially the same geometry is

$$\mathbf{M}_{\text{res}} = 24 \Delta M_{\text{res}} \quad (113)$$

The torsional stiffness may be determined as

$$k_{\theta} = \frac{\mathbf{M}_{\text{res}}}{\theta} \quad (114)$$

Substituting from equations (111)-(113) into equation (114) one finds

$$k_{\theta} = 24 \frac{EA}{\ell} \left(\frac{10 \text{ m}}{10.06 \text{ m}} \right)^2 (0.746 \text{ m})^2 \quad (115)$$

The fundamental frequency of vibration for torsional motion of the feed device may be estimated as

$$f_{\theta} = \frac{1}{2\pi} \sqrt{\frac{k_{\theta}}{M_{\text{feed}} r_g^2}} \quad (116)$$

Substituting from equations (71) and (115) into (116), it can be shown that

$$f_{\theta} = \left[\frac{1}{2\pi} \sqrt{\frac{24\pi E}{\ell M_{\text{feed}}} \left(\frac{10 \text{ m}}{10.06 \text{ m}} \right) \left(\frac{0.75 \text{ m}}{r_g} \right)} \right] r \quad (117)$$

Using the numerical values $E = 227.5 \times 10^9 \text{ N/m}^2$, ℓ from equation (102), $M_{\text{feed}} = 300 \text{ kg}$, and $r_g = 0.5 \text{ m}$, equation (117) may be rewritten as

$$f_{\theta} = (17,900 \text{ Hz/m}) r \quad (118)$$

4.5.5 Blocked Area Ratio

For the ISBW configuration, the frontal area blocked by a single spoke is

$$A_{\text{spoke}} = 2r (10.028 \text{ m}) \quad (119)$$

Where r is the radius of a single spoke. The total blocked frontal area from 24 such spokes is

$$A_{\text{blocked}} = 24 A_{\text{spoke}} = 48r (10.028 \text{ m}) (481 \text{ m}) r \quad (120)$$

The blocked area ratio a is then

$$a = \frac{A_{\text{blocked}}}{\pi (10 \text{ m})^2} = (1.53/\text{m}) r \quad (121)$$

or, equivalently,

$$r = (0.653 \text{ m}) a \quad (122)$$

4.5.6 STRUCTURAL MASS RATIO

The mass M_{spokes} of the 24 spokes in this ISBW configuration is

$$M_{\text{spokes}} = 24\rho A\ell = 24\pi r^2\rho\ell \quad (123)$$

Using the numerical values $\rho = 1740 \text{ kg/m}^3$, and $\ell = 10.06 \text{ m}$ from equation (102), it can be shown that

$$M_{\text{spokes}} = (1.32 \times 10^6 \text{ kg/m}^2) r^2 \quad (124)$$

4.5.6.1 ADDED RIM MASS DUE TO INDUCED RIM COMPRESSION

The total mass of the feed structure must, however, include the mass of added reinforcement to the rim structure within the sunshade. This is because the pretension required to obtain 20 Hz local string frequency results in a substantial compression in the rim structure. If this compression becomes excessive, it will result in local strut buckling in the rim (Out-of-plane ring buckling is unlikely due to the support provided by the sunshield support structure).

The nominal strut design parameters for the rim call for struts with a length of 2 m, radius of 3 cm, wall thickness of 1 mm, and modulus of elasticity of $227.5 \times 10^9 \text{ N/m}^2$. The corresponding Euler buckling load of a single strut is then

$$P_{\text{EU}} = 47.6 \text{ kN} \quad (125)$$

The net radial force T_1 on each joint of the rim may be expressed in terms of the spoke tension force T_0 as (see Figure 4-16)

$$T_1 = 2 \left(\frac{10 \text{ m}}{10.06 \text{ m}} \right) T_0 = 1.989 T_0 \quad (126)$$

However

$$T_0 = \sigma_0 \pi r^2 \quad (127)$$

where $\sigma_0 = 282 \text{ MPa}$ is the prestress in each spoke, and r is the radius of a spoke. Substituting from equation (127) into (126), it can be shown that

$$T_1 = (1.76 \times 10^9 \text{ N/m}^2) r^2 \quad (128)$$

Furthermore, it can be shown that the compression force F_c carried by the rim in response to the radial joint force T_1 is

$$\begin{aligned} F_c &= 1.932 T_1 \\ F_c &= (3.40 \times 10^9 \text{ N/m}^2) r^2 \end{aligned} \quad (129)$$

Setting the compression force F_c from equation (129) equal to the Euler buckling load of a rim strut P_{EU} from equation (125), we find the maximum spoke radius r_{max} which may safely be supported by the unaltered rim, as

$$r_{max} = 3.74 \text{ mm} \quad (130)$$

Note that this spoke radius is extremely small, and results in a fundamental frequency of vertical vibration (from equation (108)) of

$$f_v = 3.35 \text{ Hz} \quad (131)$$

which is unacceptable for the intended application. As a result, the rim truss must be reinforced to support the loads induced by the pretensioned spokes in this ISBW configuration.

Next we determine the necessary structural mass which must be added to the rim in order to prevent strut buckling under the required spoke pretension loads. This is accomplished by scaling up the strut cross-section while maintaining the same ratio of radius to wall thickness. Note for the nominal strut design that

$$\frac{r_s}{t} = \frac{30 \text{ mm}}{1 \text{ mm}} = 30 \quad (132)$$

where r_s is the mean strut radius. Thus, we require

$$t = \frac{r_s}{30} \quad (133)$$

as the dimensions of the cross-section are increased. For a thin-walled tube, the moment of inertia may be approximated as

$$I \cong \pi r_s^3 t = \pi \frac{r_s^4}{30} \quad (134)$$

upon substitution of equation (133). Thus, the strut buckling load may be expressed as

$$P_{EU} = \frac{\pi^2 EI}{\ell^2} = \frac{\pi^3 E r_s^4}{30 \ell^2} \quad (135)$$

after substituting for ℓ from equation (134). Using the numerical values $E = 227.5 \times 10^9 \text{ N/m}^2$, and $\ell = 2 \text{ m}$, equation (135) yields

$$P_{EU} = (5.88 \times 10^{10} \text{ N/m}^4) r_s^4 \quad (136)$$

Now, requiring the strut Euler buckling load to equal the compression force F_c induced by the spoke pretension loads requires, from equations (129 and 136),

$$r_s = \left(0.490 m^2 \right)^{\frac{1}{2}} r^{\frac{1}{2}} \quad (137)$$

The mass of the modified rim m_{rim} may be expressed as

$$m_{rim} = \frac{\pi (20m)}{(2m)} m_{strut} \equiv 31.4 m_{strut} = (31.4) 2 \pi r_s t \rho \quad (138)$$

Substituting from equation (133) into (138)

$$m_{rim} = (31.4) \frac{2\pi}{30} r_s^2 \ell \rho \quad (138)$$

Substituting from equations (137 and 139)

$$m_{rim} = (31.4) \frac{2\pi}{30} (0.240m) r \ell \rho \quad (140)$$

Using the numerical values $\ell = 2 \text{ m}$ and $\rho = 1749 \text{ kg/m}^3$

$$m_{rim} = (5,500 \text{ kg/m}) r \quad (141)$$

The mass of the original unmodified rim is

$$m_{rim_0} = (31.4) 2\pi (0.03 \text{ m})(0.001 \text{ m})(2 \text{ m})(1,740 \text{ kg/m}^3) = 20.6 \text{ kg} \quad (142)$$

Thus, the net increase in rim mass Δm_{rim} may be obtained subtracting equations (142) from equation (141) to yield

$$\Delta m_{rim} = (5,500 \text{ kg/m}) r - 20.6 \text{ kg} \quad (143)$$

4.5.6.2 TOTAL STRUCTURAL MASS RATIO

The total structural mass consists of the mass of the spokes together with the additional rim mass required to prevent rim strut buckling. Adding M_{spokes} from equations (124) and Δm_{rim} from equations (143), the total structural mass of M_{struc} is obtained where

$$M_{struc} = M_{spokes} + \Delta m_{rim} = (1.32 \times 10^6 \text{ kg/m}^2) r^2 + (5,500 \text{ kg/m}) r - 20.6 \text{ kg} \quad (144)$$

Dividing by the mass of the feed device of 300 kg, we obtain the structural mass ratio μ where

$$\mu \equiv \frac{M_{struc}}{M_{feed}} = \frac{(1.3210^6 \text{ kg} / \text{m}^2) r^2 + (5,500 \text{ kg} / \text{m}) r - 20.6 \text{ kg}}{300 \text{ kg}}$$

$$\mu = \left(\frac{r}{0.0151 \text{ m}} \right)^2 + \left(\frac{r}{0.0545 \text{ m}} \right) - 0.0687 \quad (145)$$

Note that equation (145) is limited by the requirement that $\Delta m_{rim} \geq 0$, or equivalently

$$r \geq 3.74 \text{ mm} \quad (146)$$

Finally, μ may be expressed directly in terms of the blocked area ratio a by substituting from equation (122) into equation (145). Carrying this out yields

$$\mu = 1870 a^2 + 12.0 a - 0.0687 \quad (147)$$

for the range

$$a \geq 0.00573 \quad (148)$$

4.5.7 Parametric Studies

By substituting from equation (122) into equations (108) and (118), the various natural frequencies may be expressed directly in terms of the blocked area ratio a . The resulting parametric equations are

$$f_n (585 \text{ Hz}) a \quad \text{Vertical translation frequency} \quad (149)$$

$$f_n = (11,700 \text{ Hz}) a \quad \text{torsional frequency} \quad (150)$$

(Note that the natural frequencies may alternately be expressed in terms of the structural mass ration μ by using equation (147)).

It is clear from equations (149) and (150) that all ISBW configurations are governed by the vertical translation frequency requirement.

Shown in Figure 4-18 are two curves which represent the dependence of the fundamental frequency for torsion and vertical translation, respectively as functions of the blocked area ratio a . Shown along the bottom edge of the figure in an alternate scale in terms of the total structural mass ratio (including added rim mass) μ . All curves in the figure are based on the assumption that the corresponding local string frequency of each spoke is 20 Hz, which requires an initial stress of 282 MPa in each spoke. Also shown in the figure are vertical lines corresponding to contours of values for spoke radius, r .

From the governing curve for vertical translation frequency in Figure 4-18, an ISBW with a fundamental frequency of 10 Hz is seen to have a worst-case blocked area ratio of about 1.71 percent, and a corresponding structural mass ration of about 68.3 percent. The required spoke radius for this design is slightly larger than 1 cm, and the corresponding initial tension in each spoke is about 110 kN. The modified rim struts have a radius of about 5.2 cm with a wall thickness of 1.7 mm, which results in an Euler buckling load of 423 kN.

4.6 CONCLUSIONS FOR PRELIMINARY DESIGN OF A FEED SUPPORT STRUCTURE

Based on the analyses presented in the previous sections for five configurations, it appears that the design values for the 10 Hz sunshade-tripod configuration are most

favorable, as shown in the summary, Table 4-2. While several configurations are capable of providing blocked area ratios of 2 percent or less, the required structural mass ratios for these configurations vary by an order of magnitude.

The results indicate the sunshade tripod configuration is best among the alternatives considered, both in terms of minimizing blocked area ratio and also structural mass ratio. However, opportunities exist for significant improvement of the other configurations which could lead to different conclusions.

For example, the cantilever configuration assumed that the cantilever beam is in the form of a uniform thin-walled tube. Extension of these results to include a lattice beam would likely produce enhanced performance of this configuration.

In addition, the bicycle wheel configurations each require excessive mass, primarily because of the large pretensions required to assure sufficiently high local string frequencies. It should be noted that alternate rigging patterns for the spokes could well lead to significant enhancement of performance. However, all bicycle wheel designs have inherent disadvantages of unexplored magnitude due to (1) effects of complex shadow pattern on optics of the reflector, (2) vulnerability to feed misalignment due to loss of tension in any spoke, and (3) relative complexity of deployment and adjustment of spoke tensions.

SECTION 5

CONCLUDING REMARKS

For each of the four areas of PSR design concerns explored during this study, specific aspects requiring further study can be identified. Study and refinement of the deployment geometry for the Pactruss is needed to completely avoid member strain during deployment without the use of additional structures such as stand-offs.

The investigation of how structural redundancy could be reduced or eliminated in the trusses revealed that a reduction of redundancy has a profound effect on truss stiffness and sensitivity to manufacturing tolerances. This effect is not completely understood, and yet has important implications for the design of precision structures.

The sunshade is an area of PSR design that requires significant future effort. The sunshade is an extremely large structure. When one considers the amount of multilayer insulation (MLI) that such a device would require, it is seen also to be quite massive. In order to achieve appropriate fundamental frequencies and avoid unwanted control/structure interaction, careful review of the dynamic properties of MLI blankets, as well as the sunshade structural support must be performed. The sunshade design issue is essentially unexplored and may pose some of the more challenging problems for PSR technology development.

The parametric studies that were developed for the feed support structure reveal that the feed support structure may benefit from attachment to the sunshade structure. Likewise, although not yet analyzed, the sunshade may benefit from its attachment to the most promising of the FSS developed herein, the sunshade tripod.

Further investigation of these and other related issues will be made in Task 8, "Concepts and Analysis for Precision Segmented Reflectors."

REFERENCES

1. Hedgepeth, J.M., "Pactruss Support Structure for Precision Segmented Reflectors: Final Report," NASA CR-181747, Task 9, June 1989.
2. Hedgepeth, J.M. and Miller, R.K., "Investigation of Structural Behavior of Candidate Space Station Structure: Final Report," NASA CR 181746, Task 8, June 1989.
3. Pawlik, E., Lin, R. and Fichter, W.B., "NASA's Precision Segmented Reflectors (PSR) Project," SPIE Proceedings, Volume 1114, SPIE Conference, Orlando, FL, March 1989.
4. Collins, T.J. and Fichter, W.B., "Design of Support Trusses for Large PSR," SPIE Proceedings, Volume 114, pages 1114-49, SPIE Conference, Orlando, FL, March 1989.
5. Anderson, M.S. and Nimmo, N.A., "Dynamic Characteristics of Statically Determinate Space-Truss Platforms," Paper 85-0819, 26th AIAA/ASME/ASCE/AHS Structures, Structural Dynamics and Materials Conference, Orlando, FL, April 15-17, 1985.
6. Hedgepeth, J.M., "Application of High-Fidelity Structural Deployment Analysis to the Development of Large Deployable Trusses," IAF-89-339, 40th Congress of the International Astronautical Federation, Malaga, Spain, October 7-12, 1989.

TABLE 3-1: RESULTS OF MONTE CARLO RUNS

N = 100, Strain RMS = 1×10^{-5}

20-Meter Five-Ring LDR Trusses

		RMS ERRORS		TILT
		Average	Worst Case	
<u>Pactruss:</u>	Full No circum.	40.1 μm 79.8	70.8 μm 165.9	< 85 < 110
<u>Tetratruss:</u>	Full Determinate	42.6 152.0	73.2 328.0	< 80 < 90

TABLE 4-1: RESTORING MOMENT CREATED BY INDIVIDUAL WIRES FOR ROTATIONS SHOWN IN FIGURE 4-13 FOR RSBW CONFIGURATION

Point No.	\underline{e}	\underline{u} (m)	δ (m)	ΔT	Restoring Moment
1-Upper	(0.0, 0.0808, -0.9967)	(0.75, 0, 0) θ	0	0	0
2-Upper	(-0.4984, 0.0808, -0.8632)	(0.75, -0.375, 0) θ	-0.4041 θ	$(-0.4041 m) \frac{EA-\theta}{l}$	$(0.4041 m)^2 (\frac{EA}{l})\theta$
3-Upper	(-0.8632, 0.0808, -0.4984)	(0.75, -0.65, 0) θ	-0.6999 θ	$(-0.6999 m) \frac{EA-\theta}{l}$	$(0.6999 m)^2 (\frac{EA}{l})\theta$
4-Upper	(-0.9967, 0.0808, 0.0)	(0.75, -0.75, 0) θ	-0.8081 θ	$(-0.8081 m) \frac{EA-\theta}{l}$	$(0.8081 m)^2 (\frac{EA}{l})\theta$
1-Lower	(0.0, -0.0808, -0.9967)	(-0.75, 0, 0) θ	0	0	0
2-Lower	(-0.4984, 0.0808, -0.8632)	(-0.75, -0.375, 0) θ	0.4041 θ	$(0.4041 m) \frac{EA-\theta}{l}$	$(0.4041 m)^2 (\frac{EA}{l})\theta$
3-Lower	(-0.8632, -0.0808, -0.4984)	(-0.75, -0.65, 0) θ	0.6999 θ	$(0.6999 m) \frac{EA-\theta}{l}$	$(0.6999 m)^2 (\frac{EA}{l})\theta$
4-Lower	(-0.9967, -0.0808, 0.0)	(-0.75, -0.75, 0) θ	0.8081 θ	$(0.8081 m) \frac{EA-\theta}{l}$	$(0.8081 m)^2 (\frac{EA}{l})\theta$

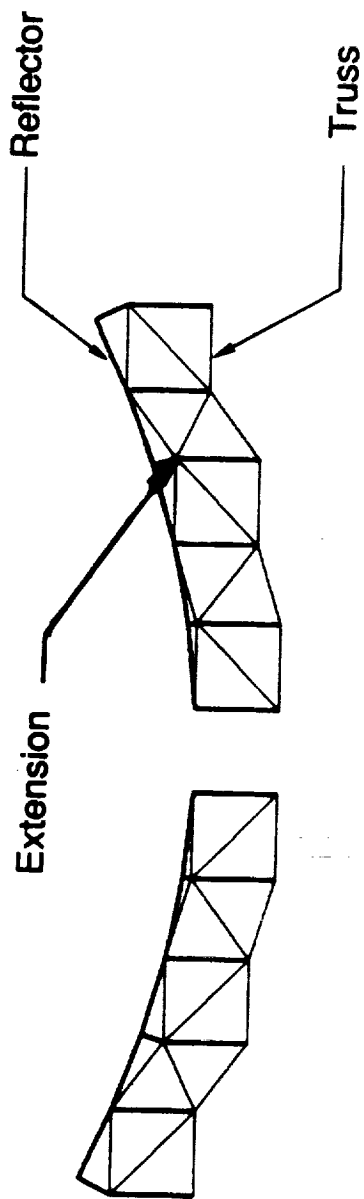
TABLE 4-2: COMPARISON OF DESIGN PARAMETERS FOR 10 HZ FEED SUPPORT STRUCTURES OF VARIOUS CONFIGURATIONS

Configuration	Blocked Area Ratio, α (%)	Structural Mass Ratio, μ (%)
Cantilever ⁽¹⁾	6.4	46
Rim-Tripod ⁽¹⁾	2.0	15
Sunshade-Tripod ⁽¹⁾	1.7	11
Radial Spoke Bicycle Wheel ⁽²⁾	2.3	120 ⁽³⁾
Interlaced Spoke Bicycle Wheel ⁽²⁾	1.7	68

(1) Minimum wall thickness of 1 mm used in design

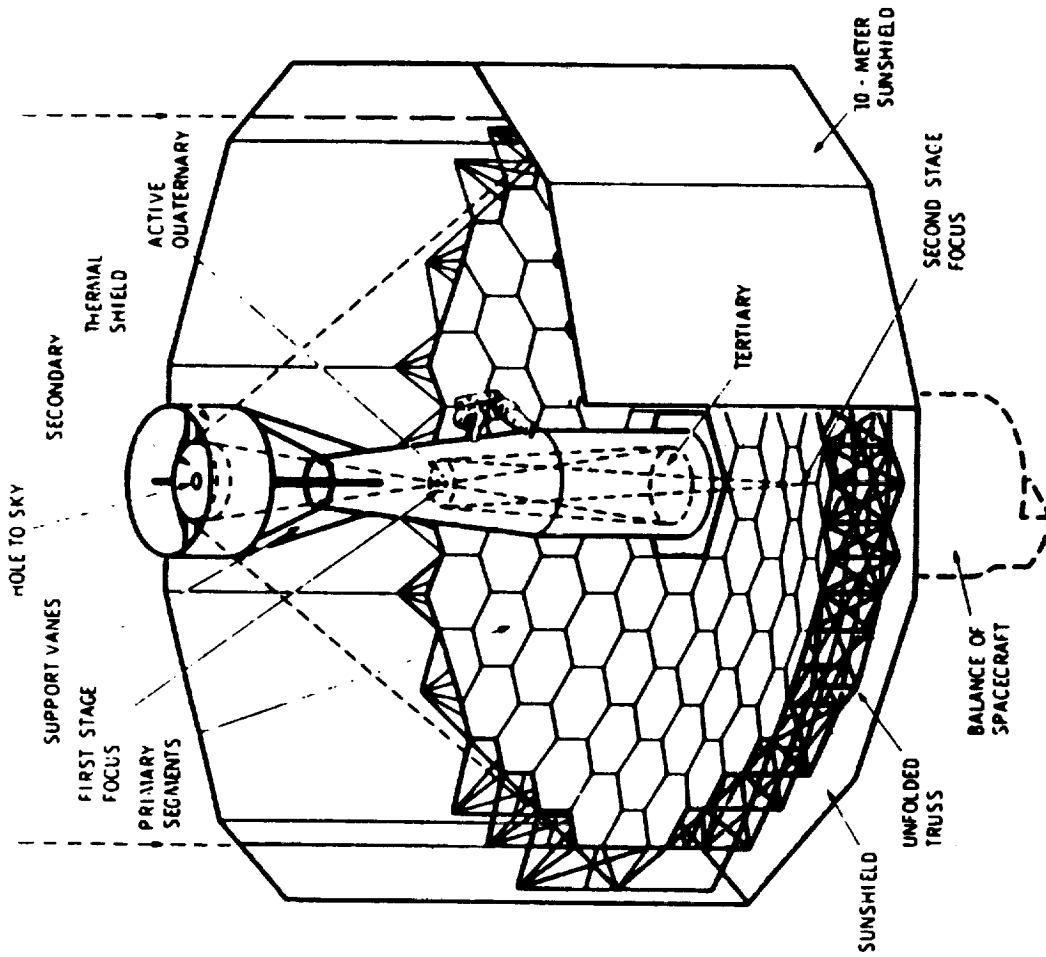
(2) Sufficient pretension to provide local string frequency of 20 Hz in spokes used in design

(3) This structural mass estimate is overly optimistic since the added mass of necessary rim reinforcement is neglected



Deployed

Figure 1-1. Design to avoid pop-through.



Cutaway Perspective

Figure 2-1. Application of PACTRUS to LDR.

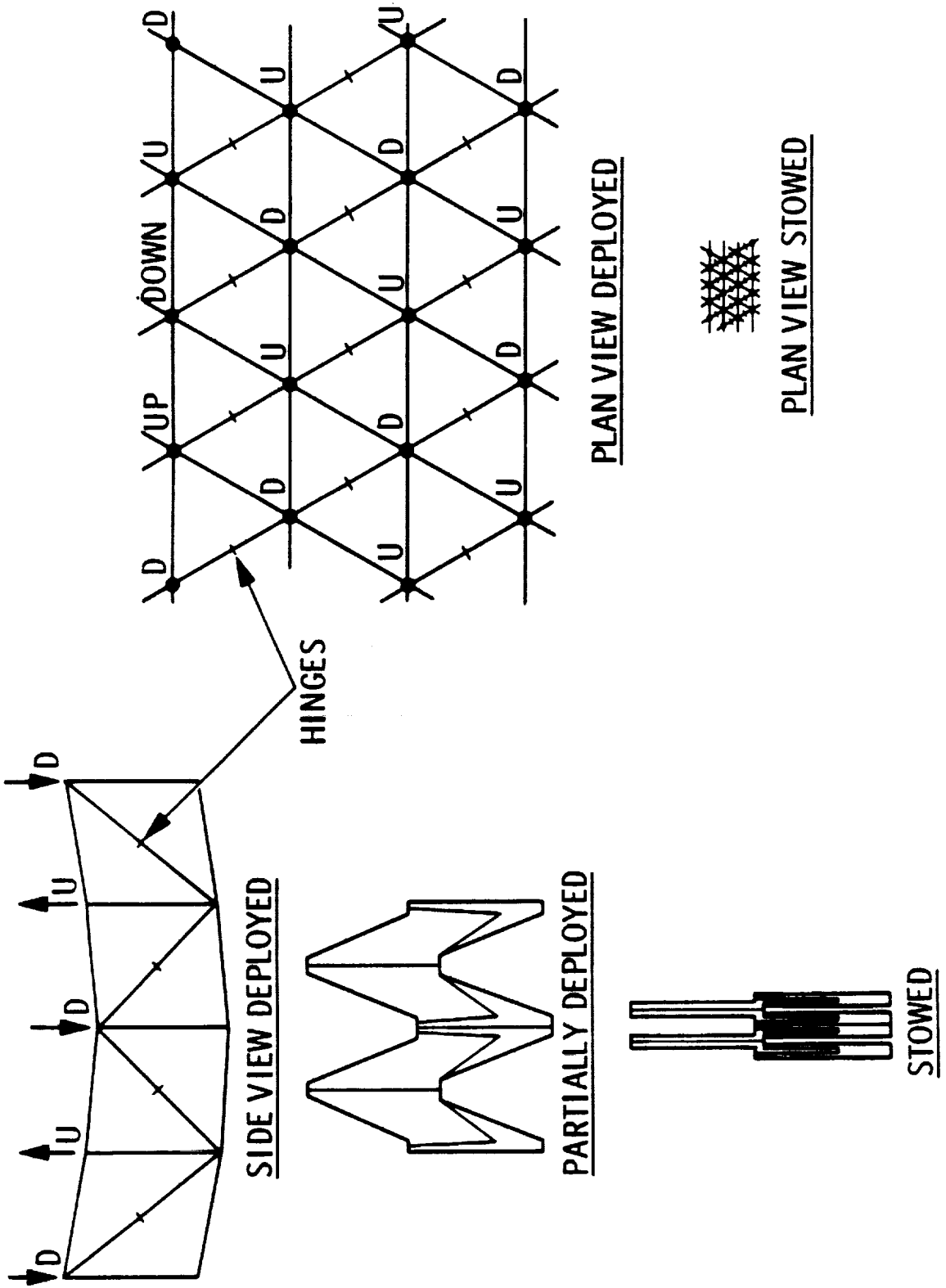


Figure 2-2. Pactruss concept.

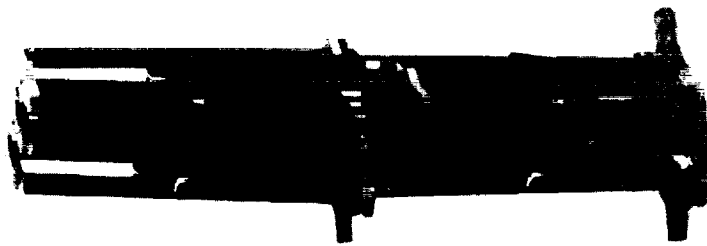
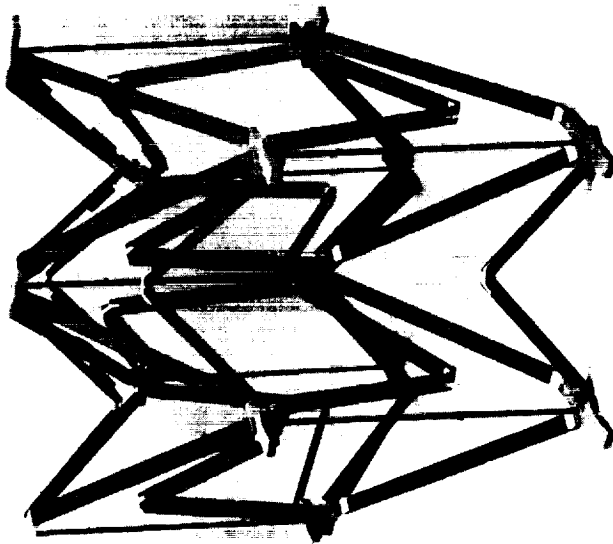
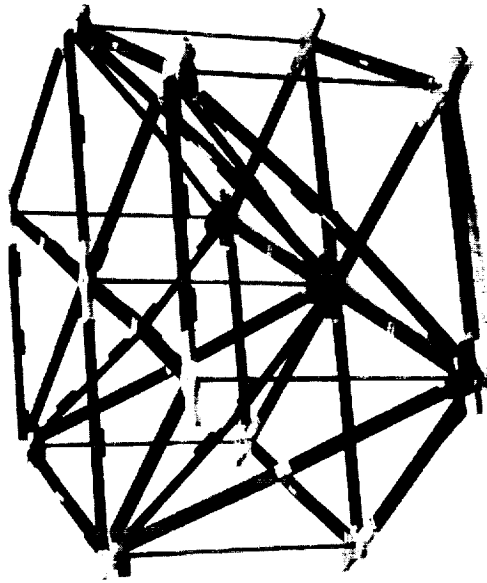


Figure 2-3. Triangular Truss.

ORIGINAL PAGE
BLACK AND WHITE PHOTOGRAPH

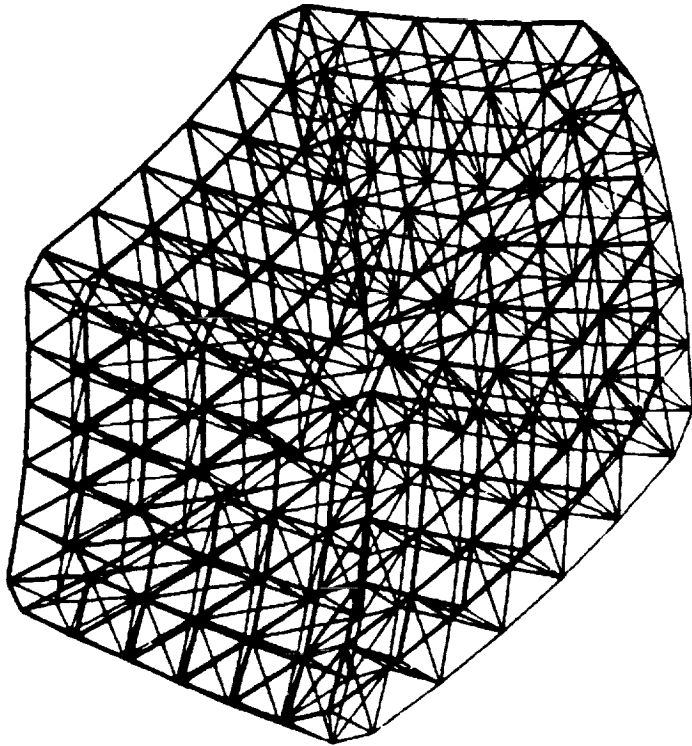
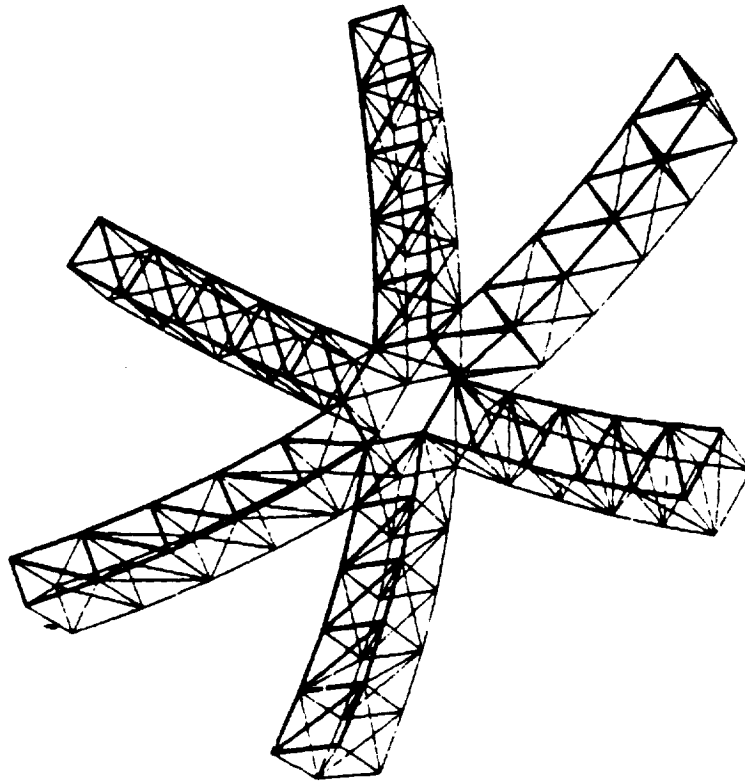
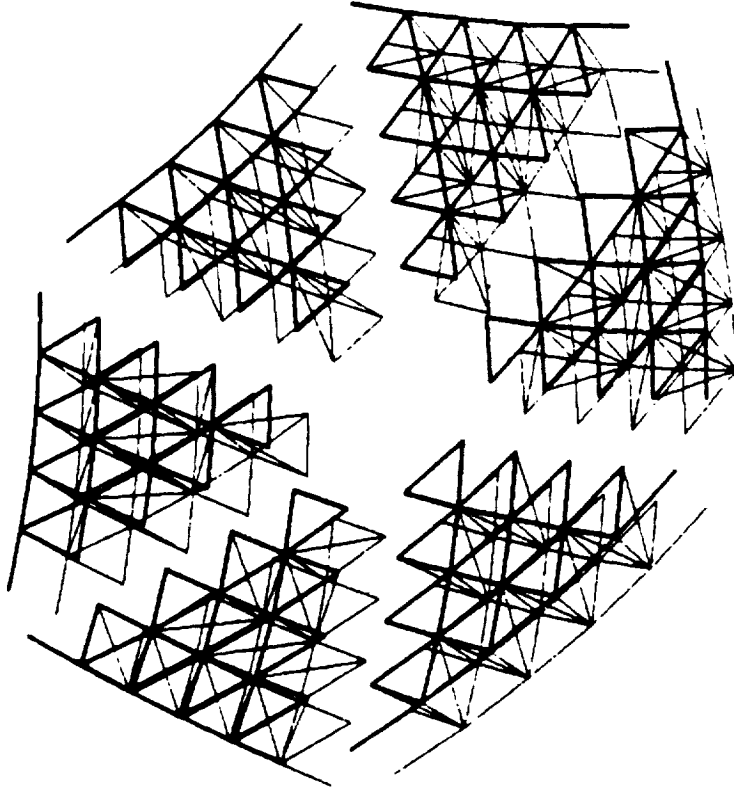


Figure 2-4. Hybrid Pactruss.

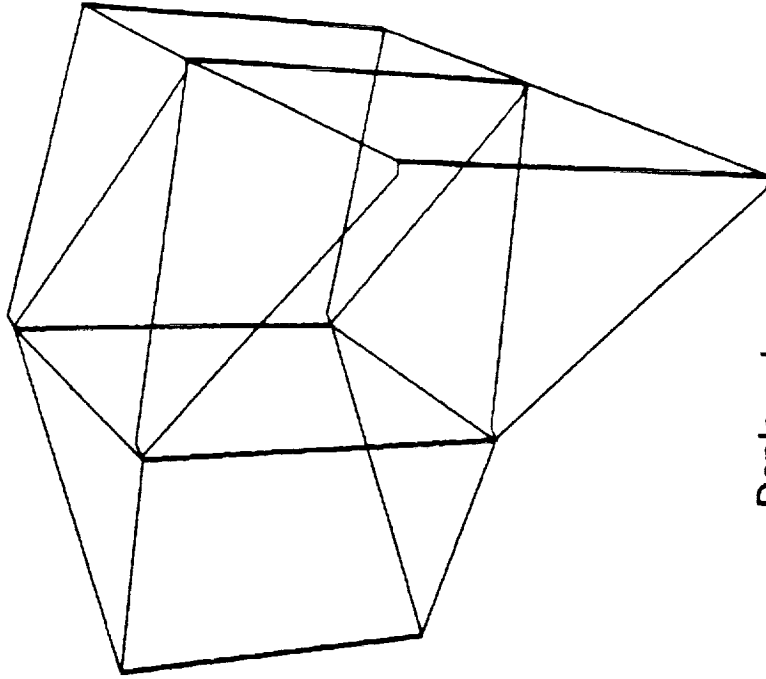
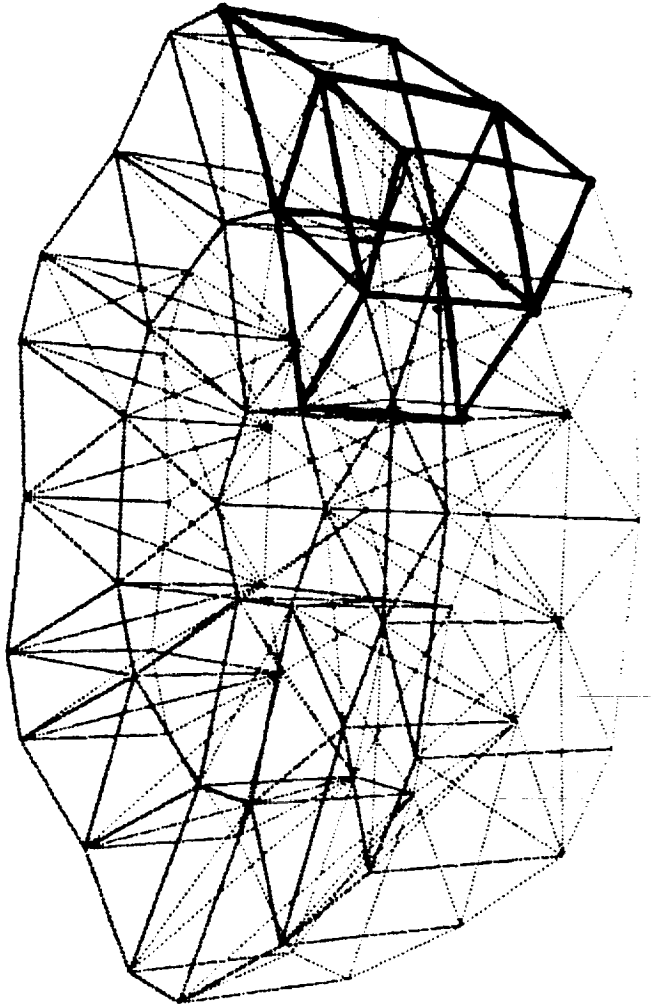


Single-fold beams



Pactruss

Figure 2-5. Parts of hybrid Pactruss.



Deployed

Figure 2-6. XGTEST.

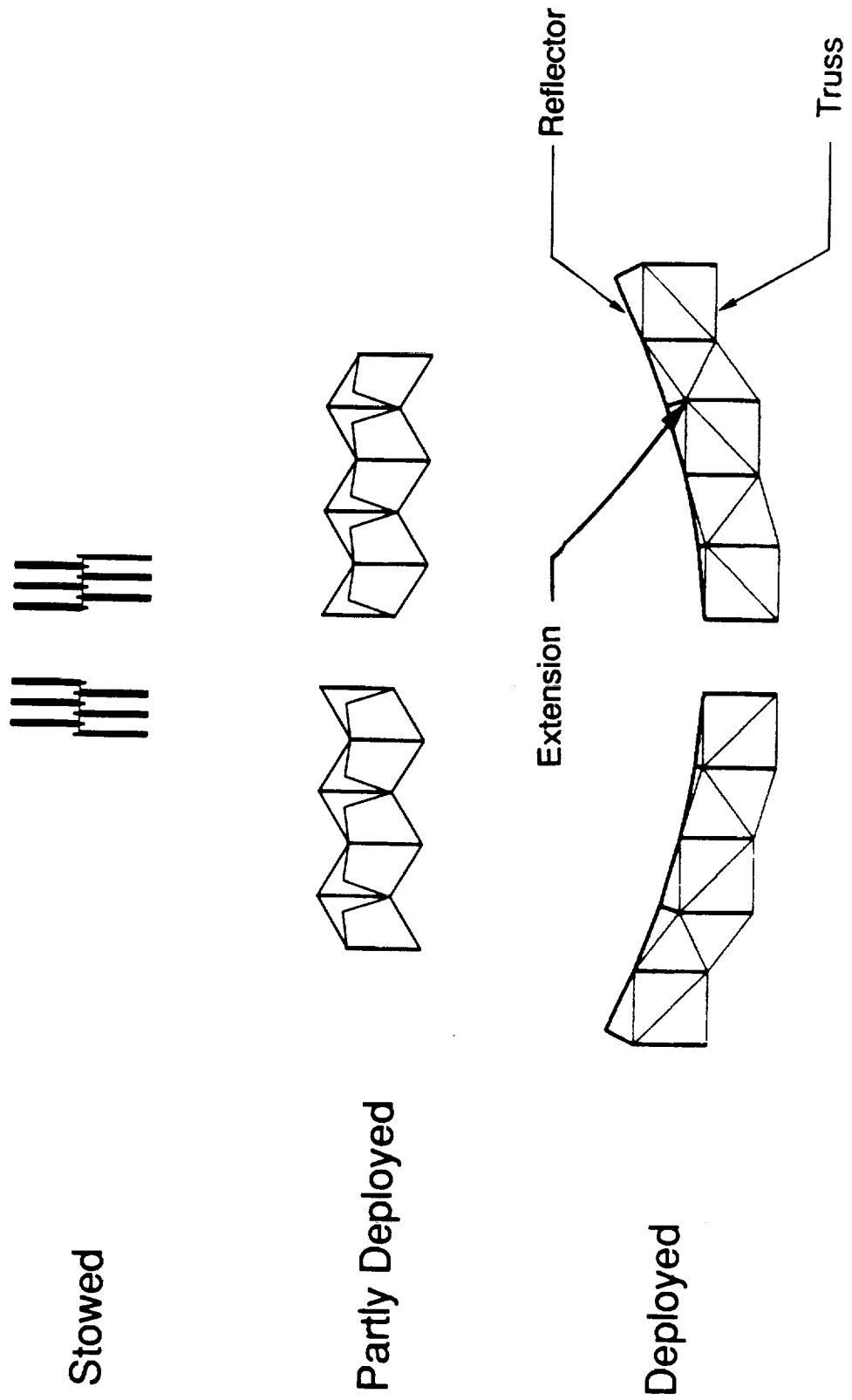
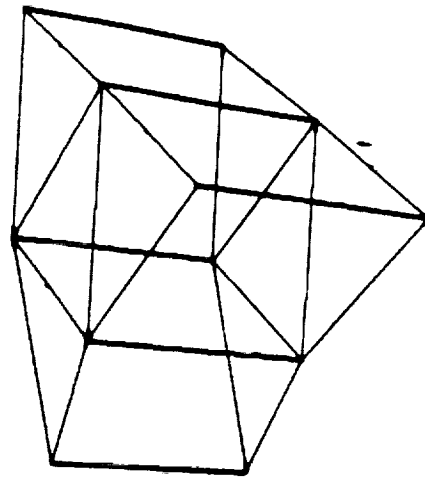
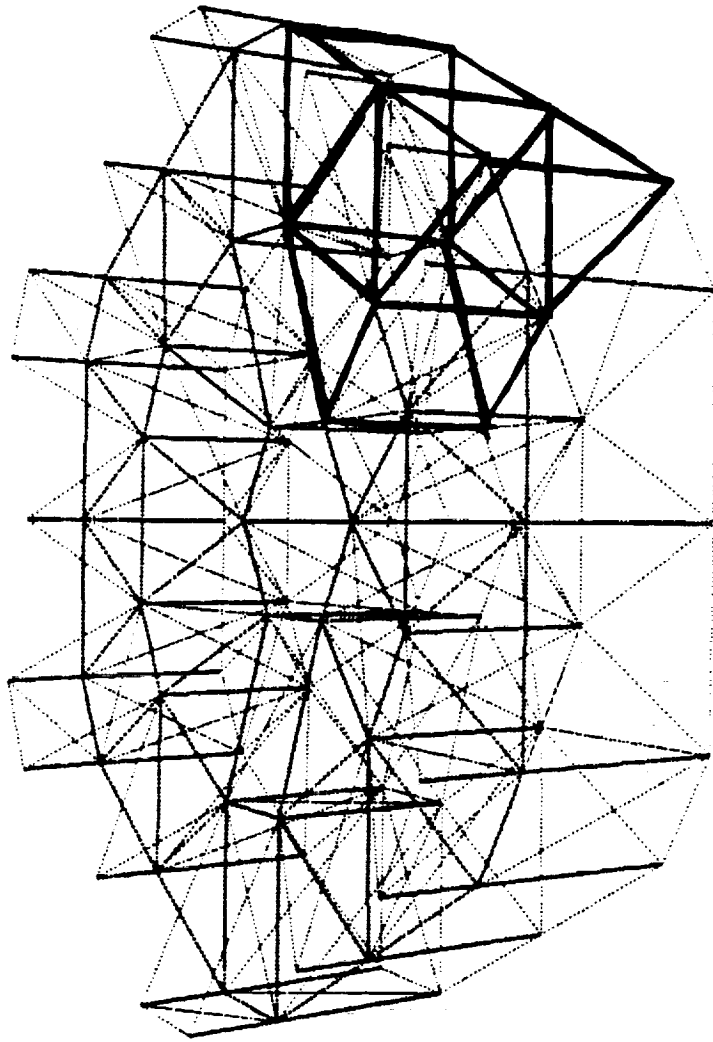


Figure 2-7. Design to avoid pop-through.



Deployed

Figure 2-8. XGTK.

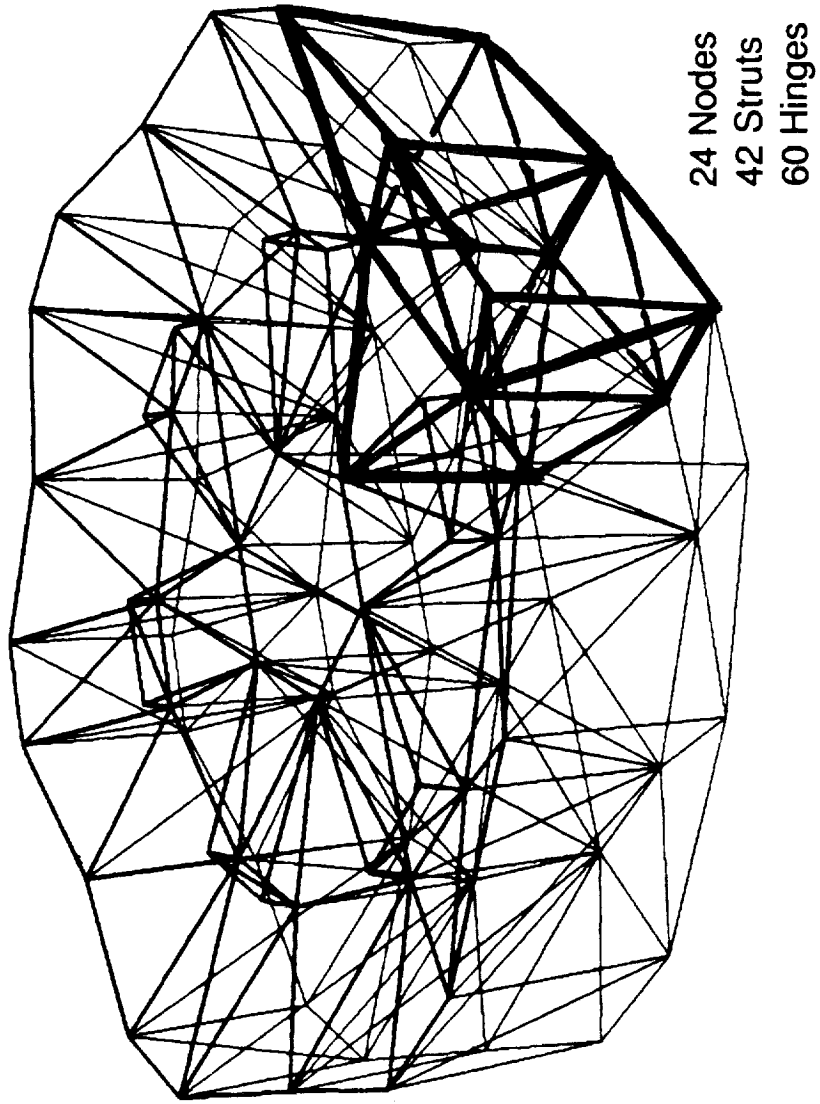


Figure 2-9. HEXPAK.

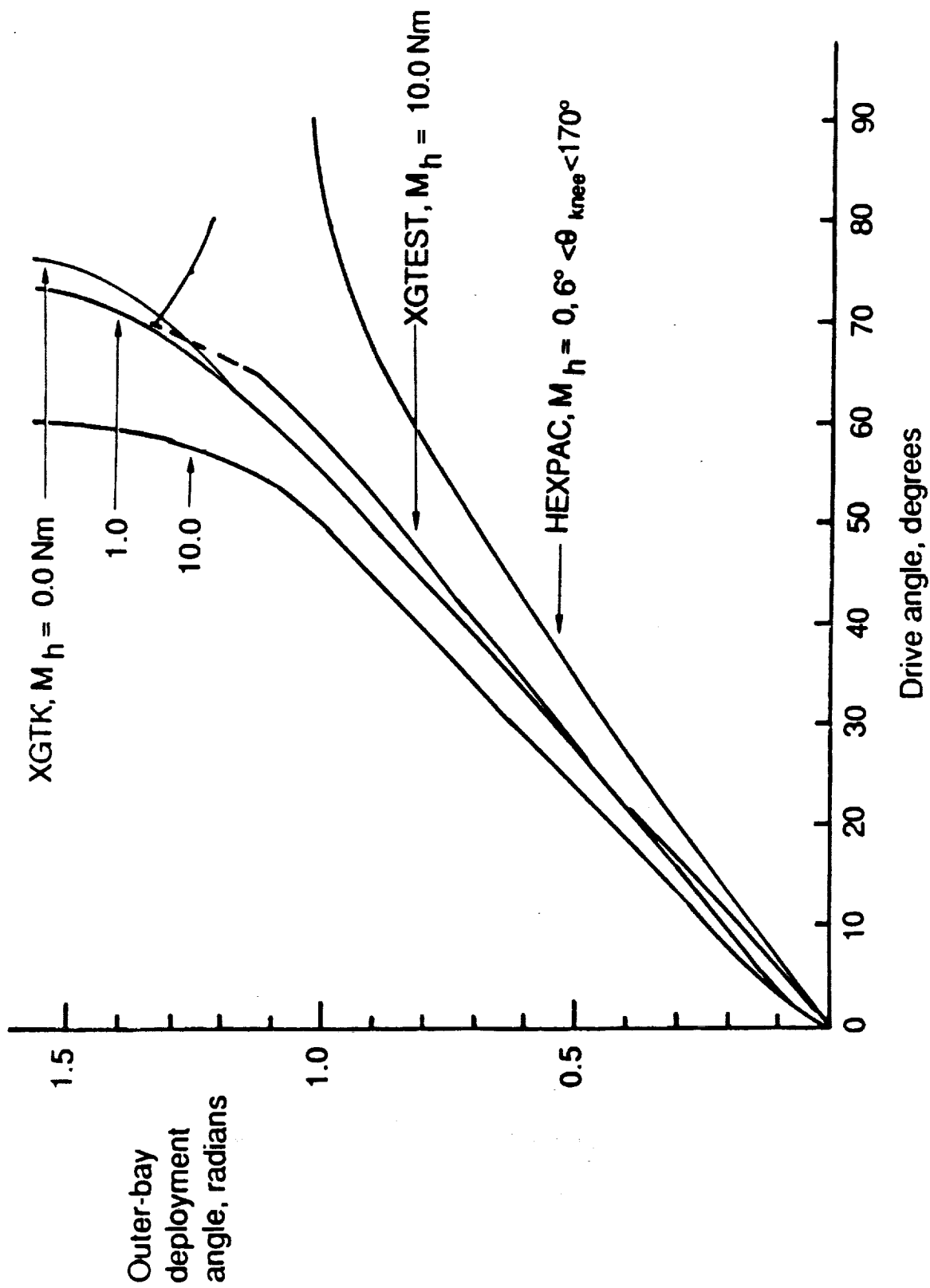


Figure 2-10. Deployment angle of outer bay.

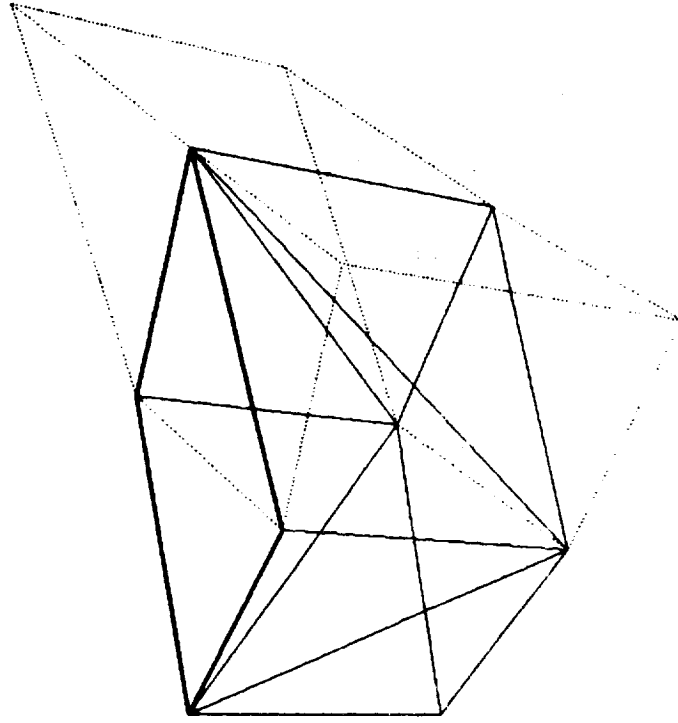


Figure 2-11. Deployment analysis model for the case without circumferentials.

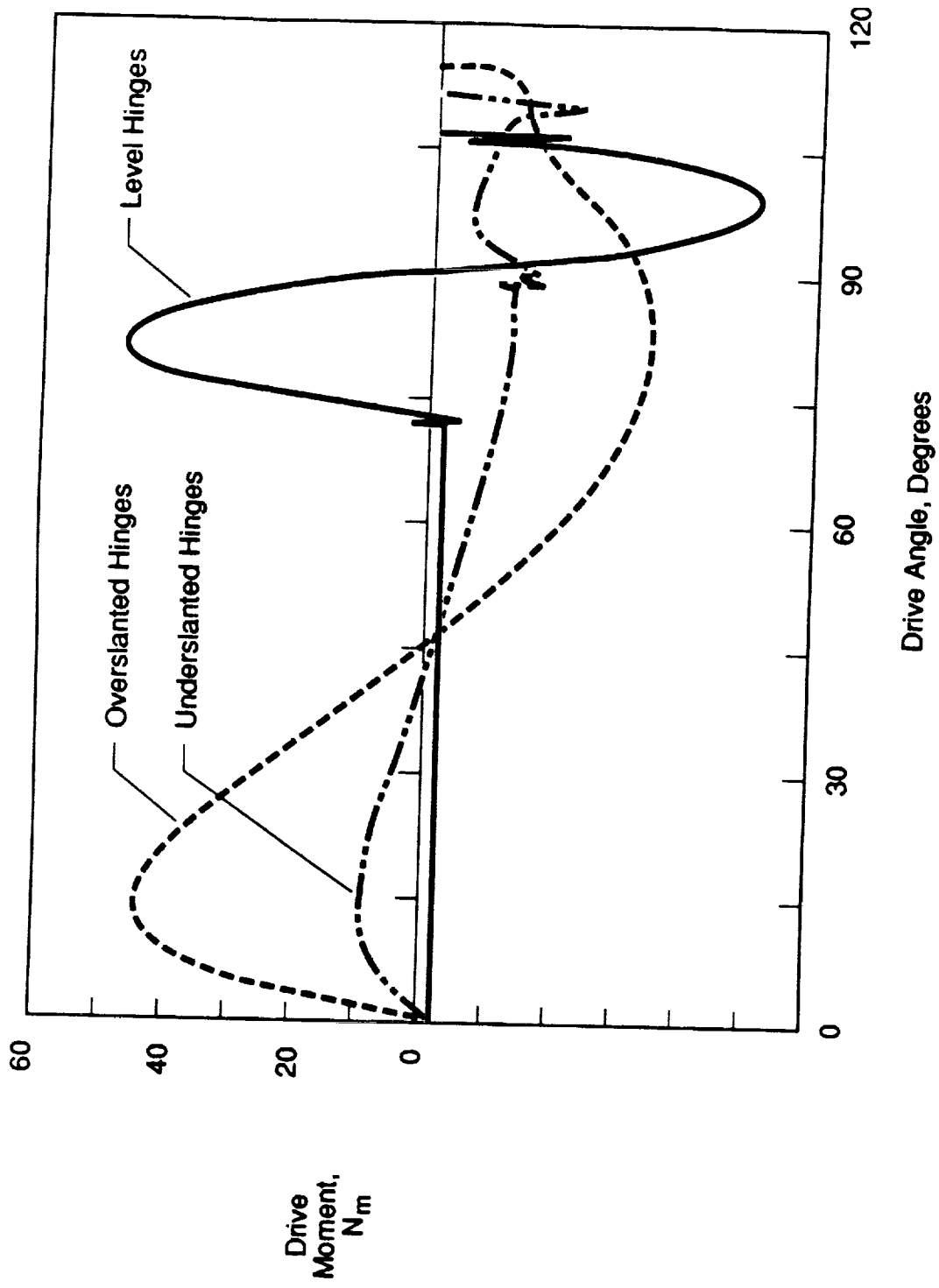


Figure 2-12. Deployment without circumferentials, outer bay drive.

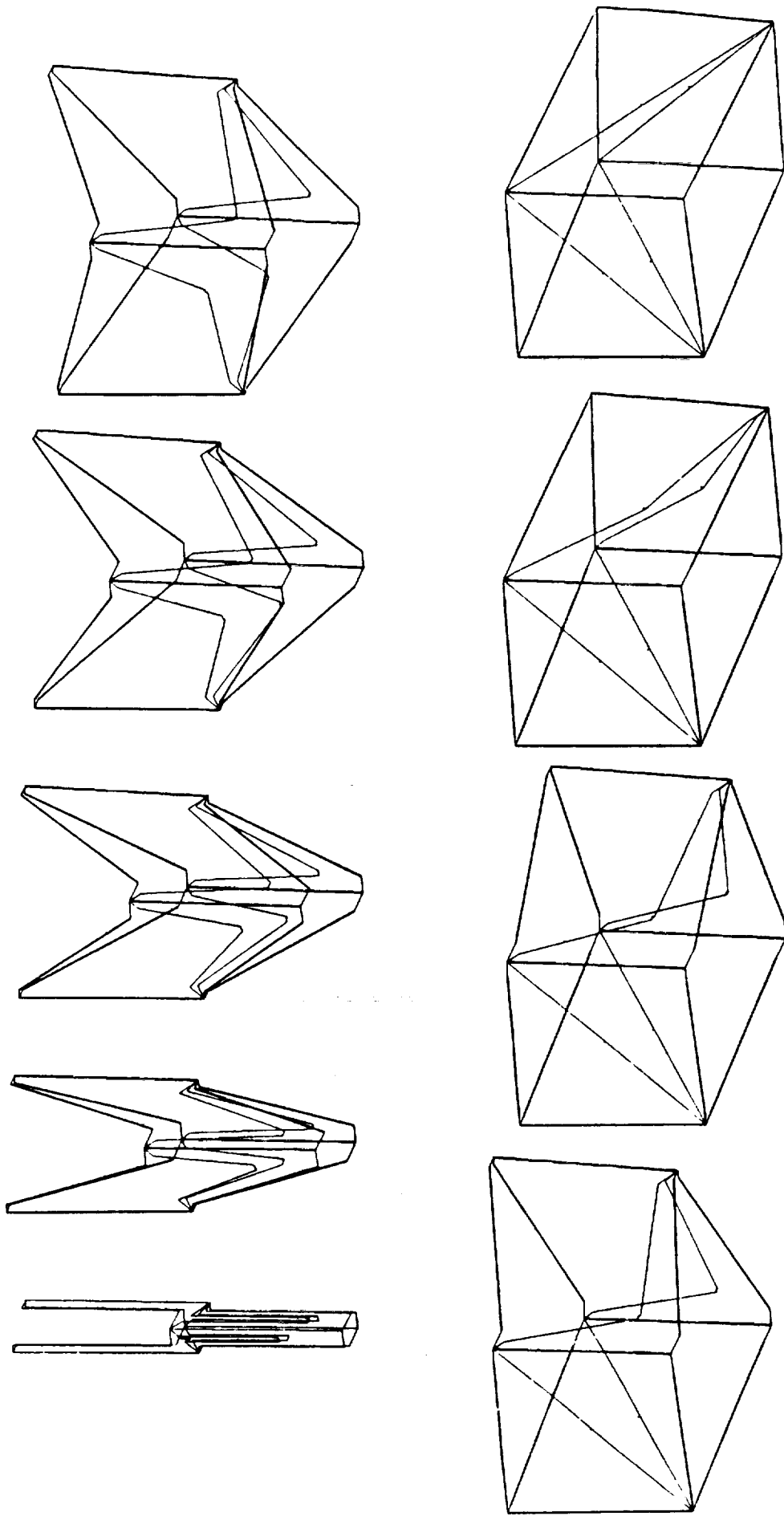
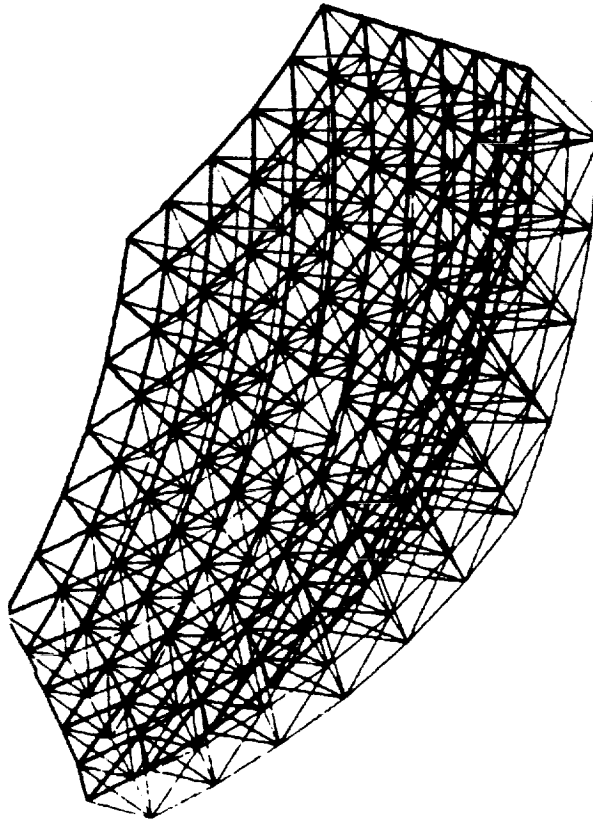
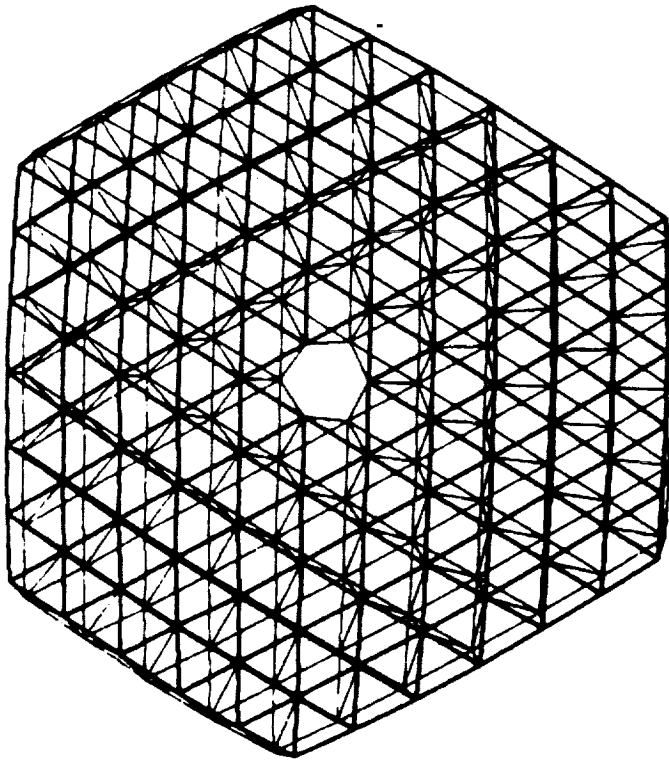
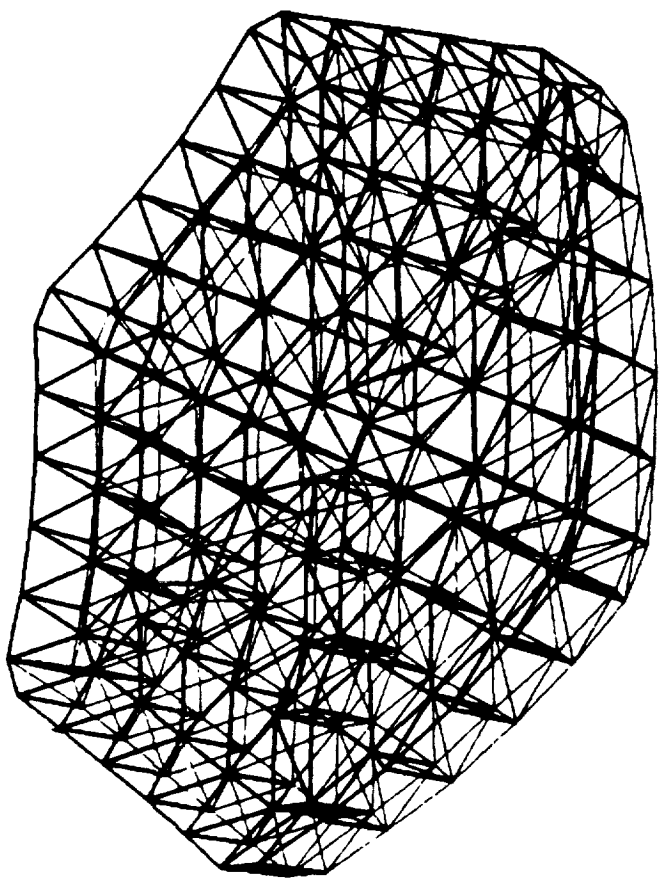
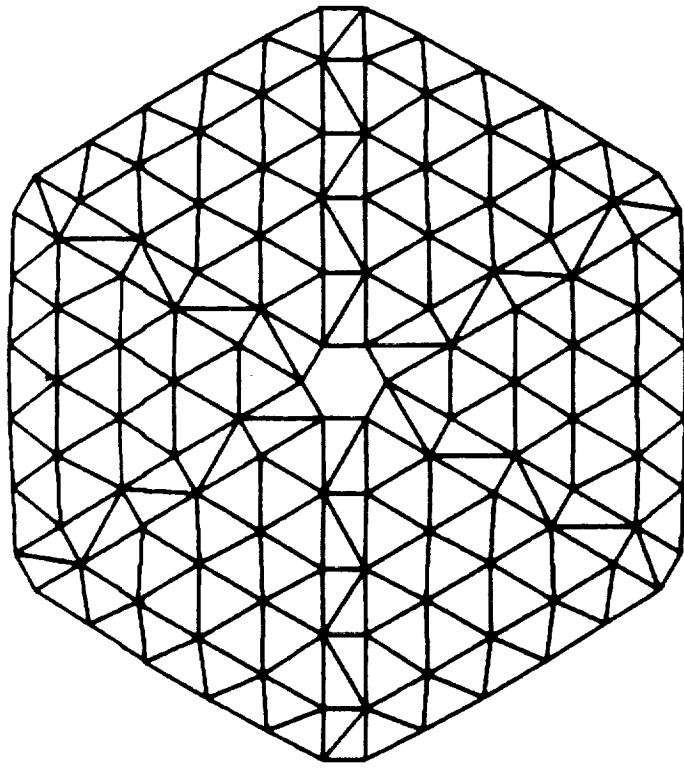


Figure 2-13. Deployment sequence for model without circumferentials.



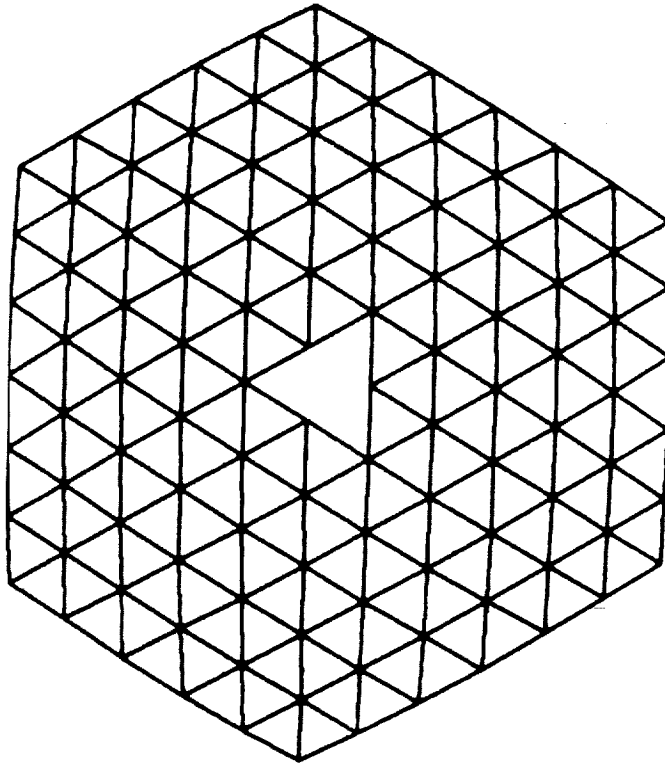
198 Nodes
789 Struts
291 Redundants

Figure 2-14. Five-ring tetrahedral truss.

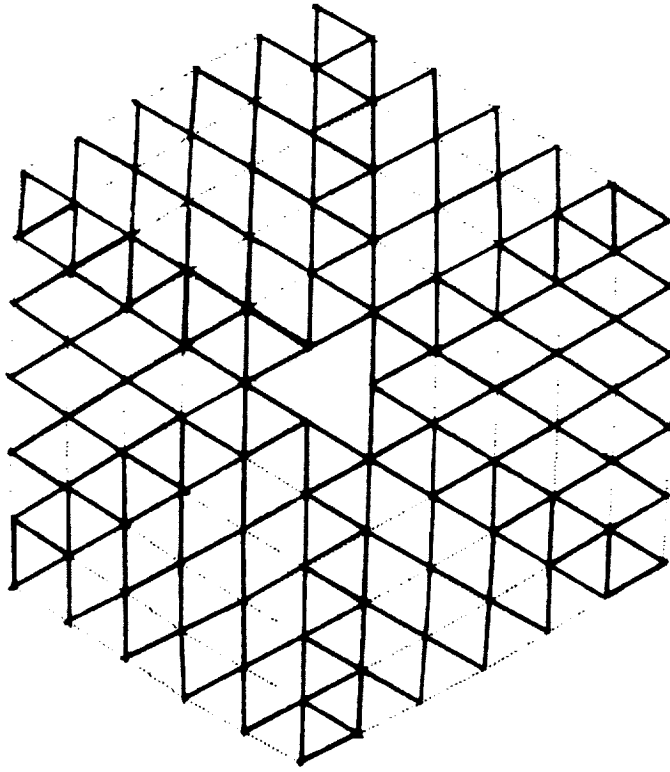


252 Nodes
1014 Struts
264 Redundants

Figure 2-15. Five-ring PACTRUSS.

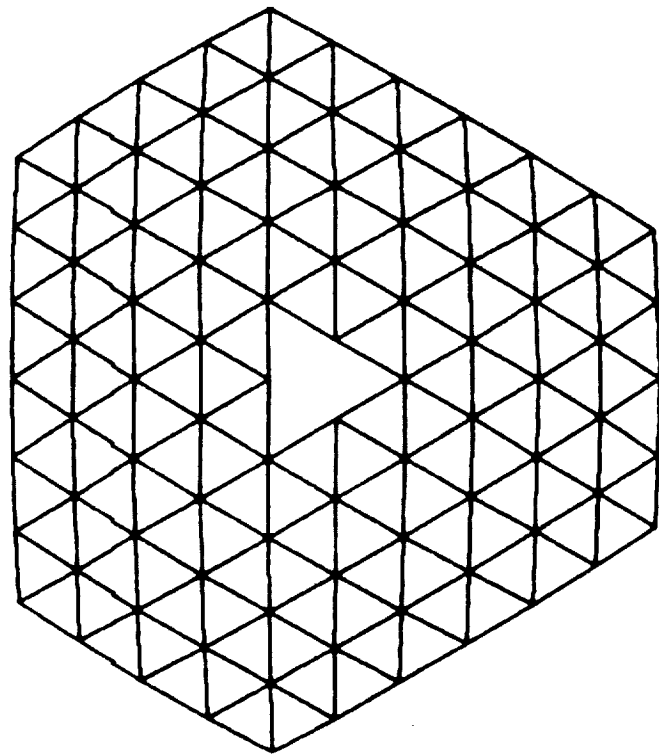


Full Truss
285 Struts



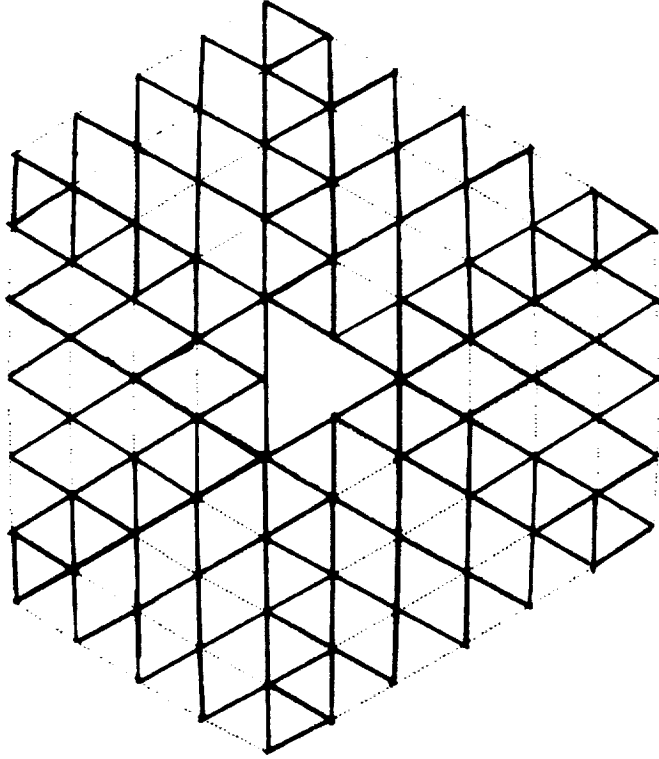
75 Redundants
Eliminated

Figure 2-16a. Tetrahedral truss upper surface.



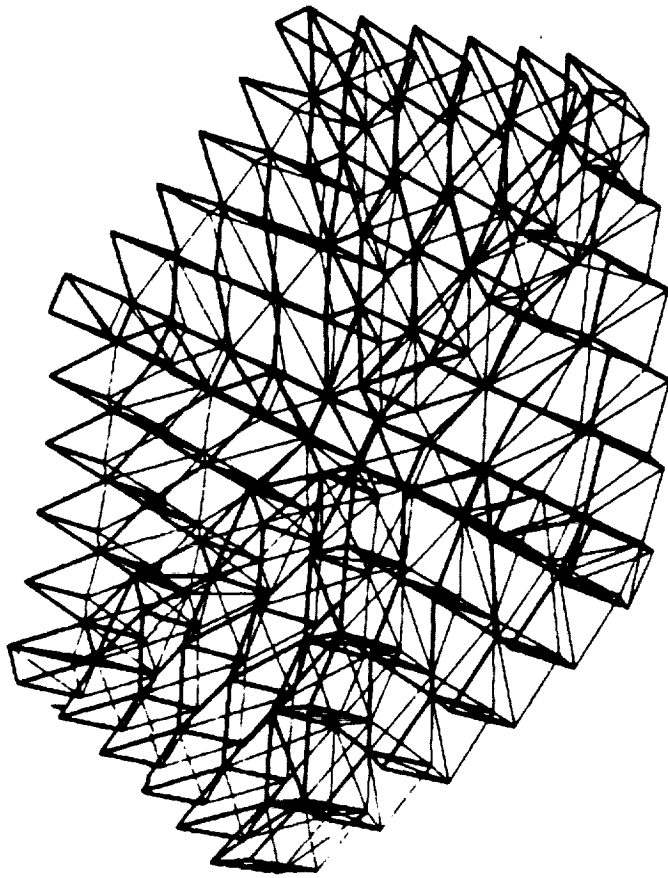
Full Truss
234 Struts

66 Core Redundants
Removed



60 Redundants
Eliminated

Figure 2-16b. Tetrahedral truss lower surface.



198 Nodes
609 Struts
111 Redundants
294 Redundants removed

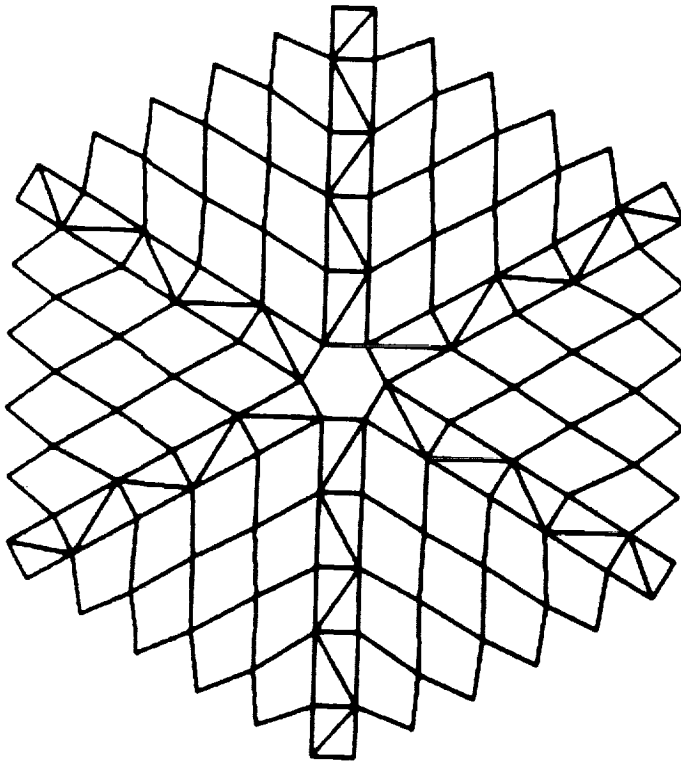


Figure 2-17. Simplified PACTRUSS.

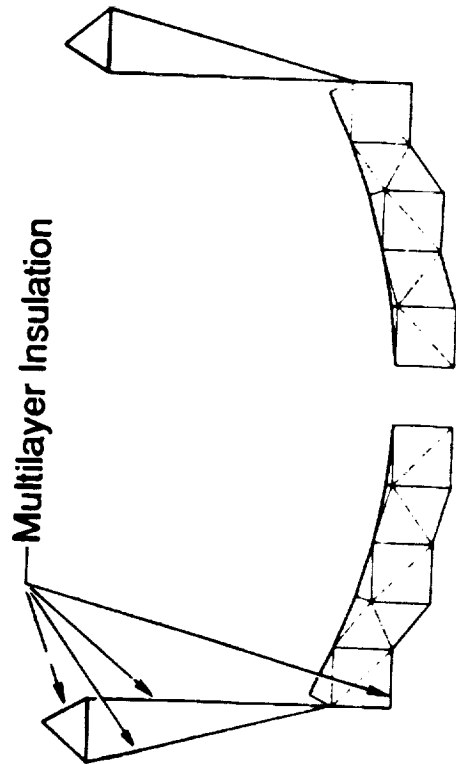
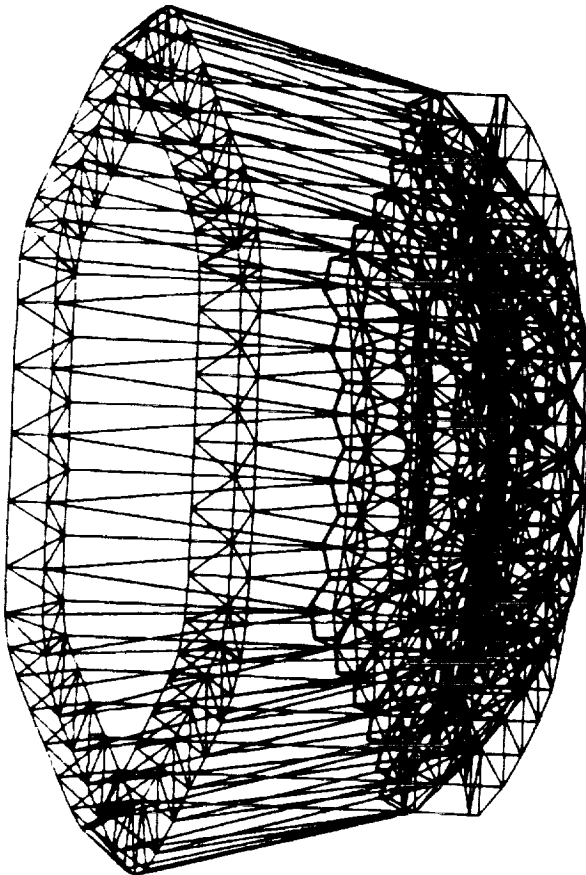
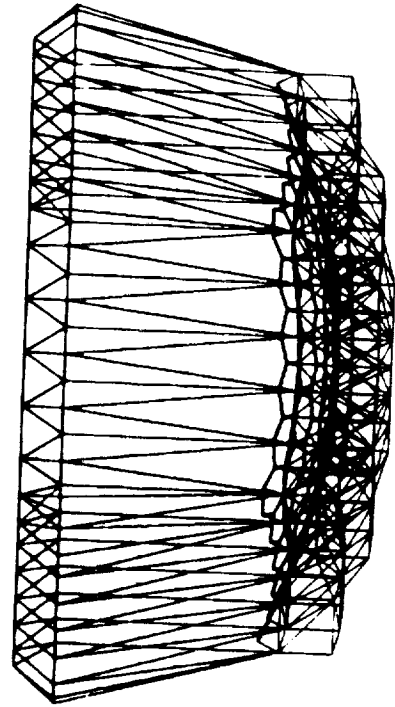
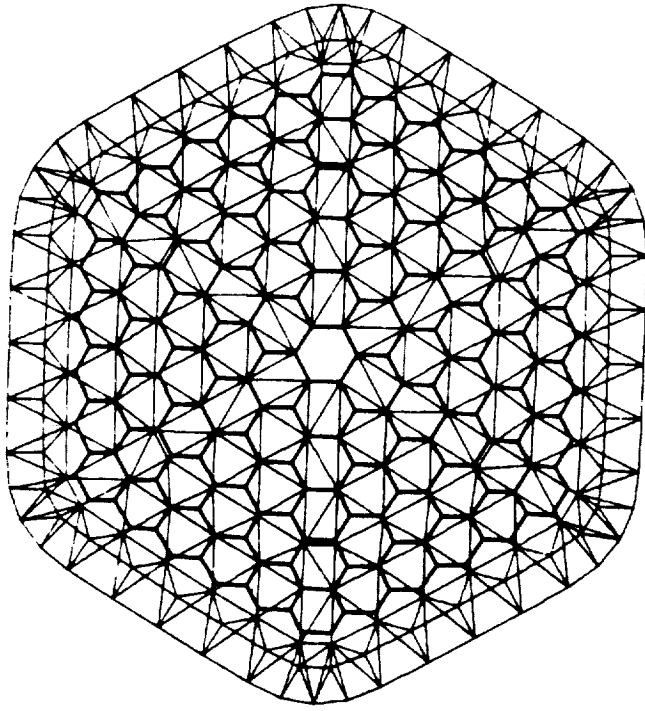


Figure 3-1. Deployable support truss and sunshade.

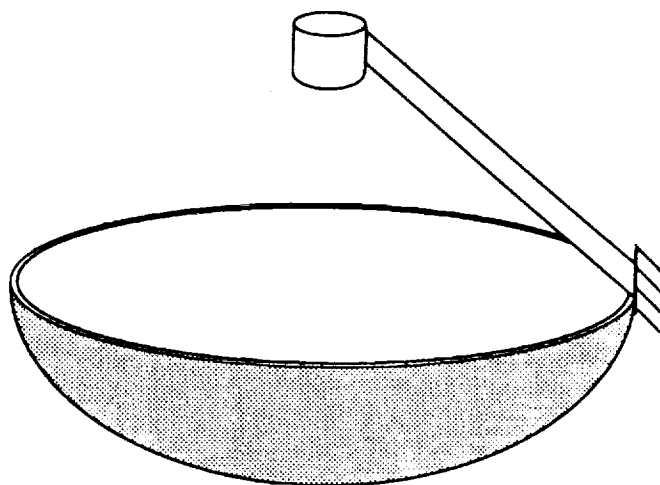


Figure 4-1. Cantilever configuration of feed support structure.

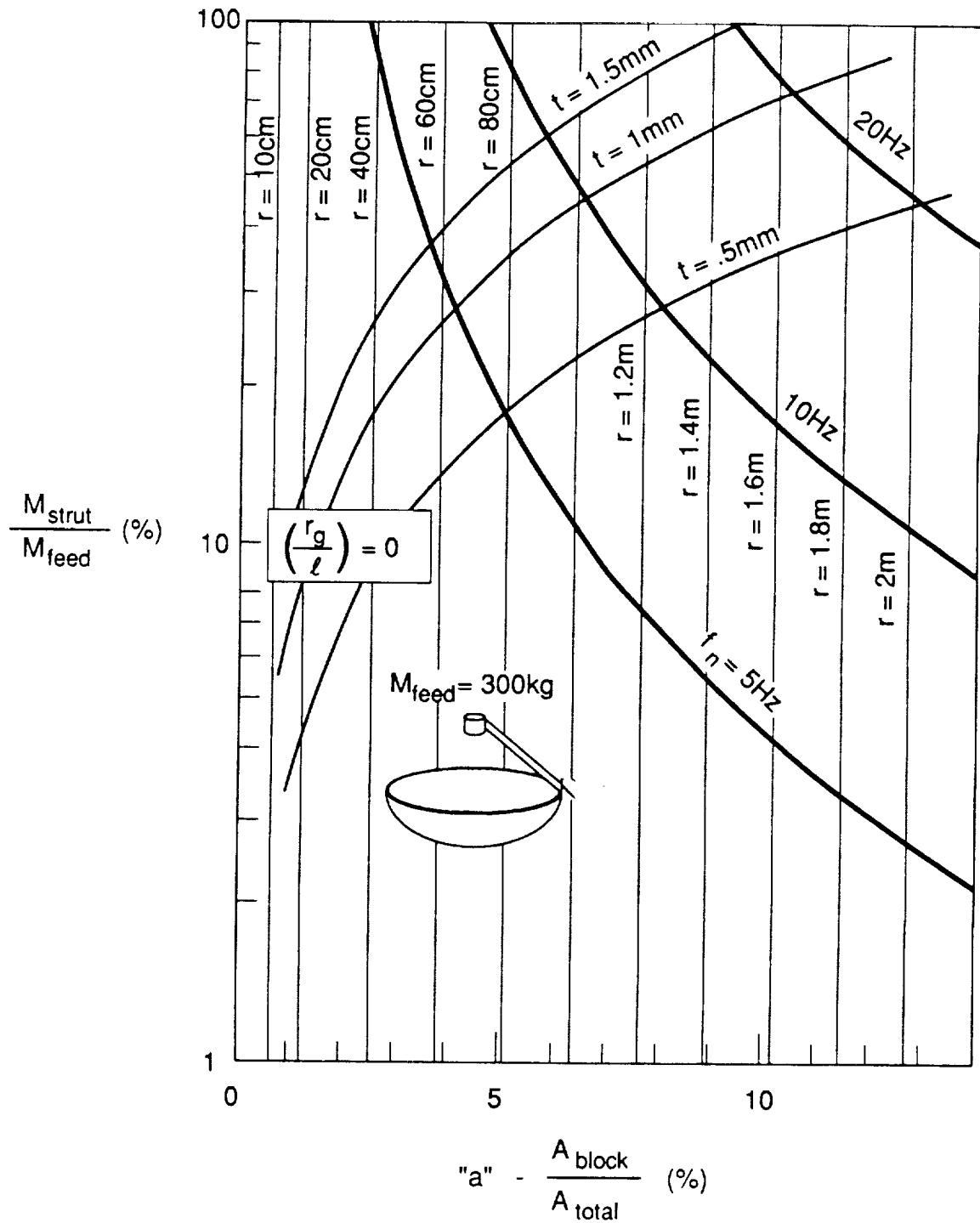


Figure 4-2. Feed support mass ratio μ versus assigned values of blocked area ratio, "a," fundamental vibration frequency, f_n , and radius of gyration, r_g , for the cantilever configuration.

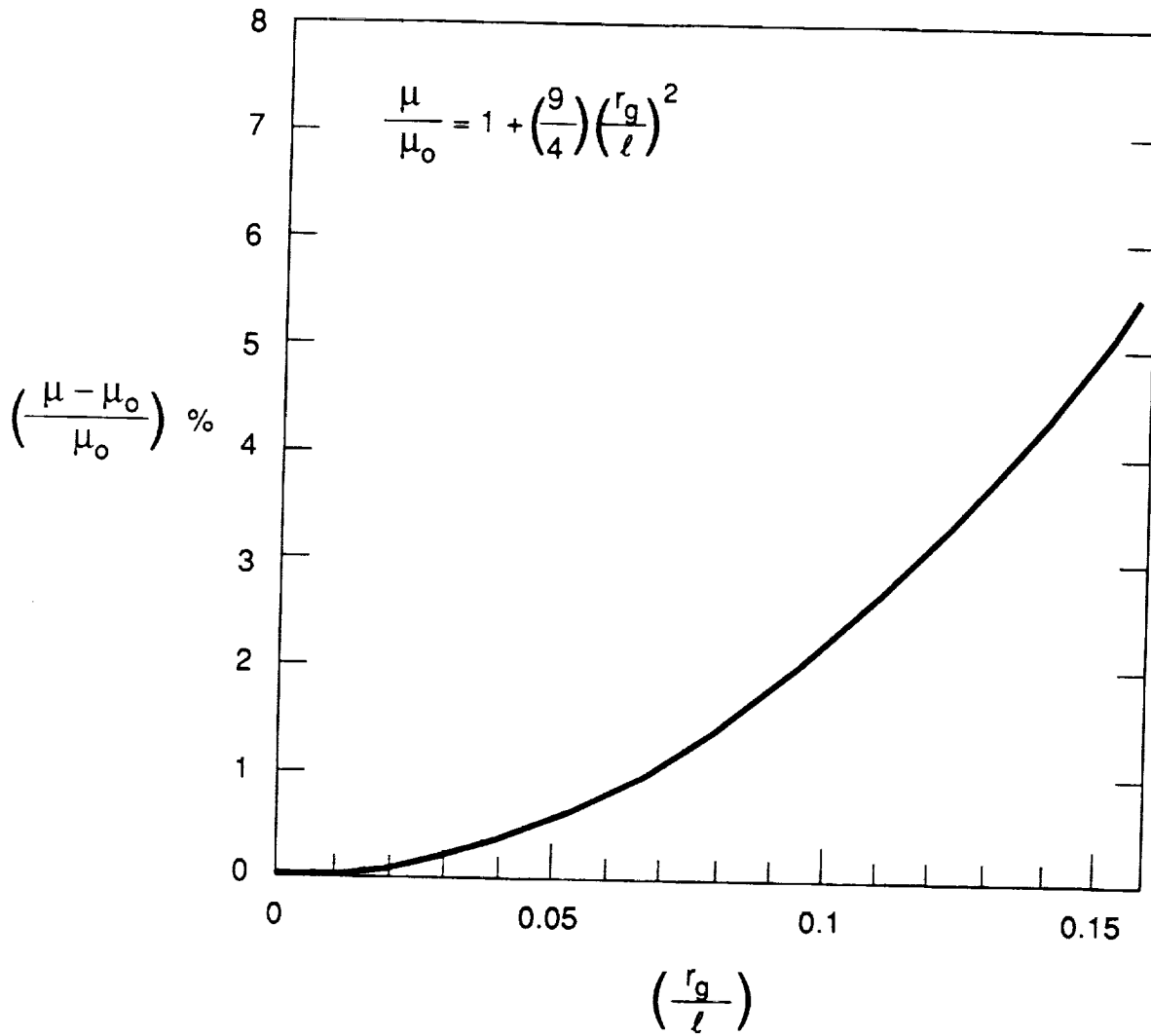


Figure 4-3. Effect of radius of gyration of feed mass on required mass ratio μ for fixed natural frequency and blocked area ratio.

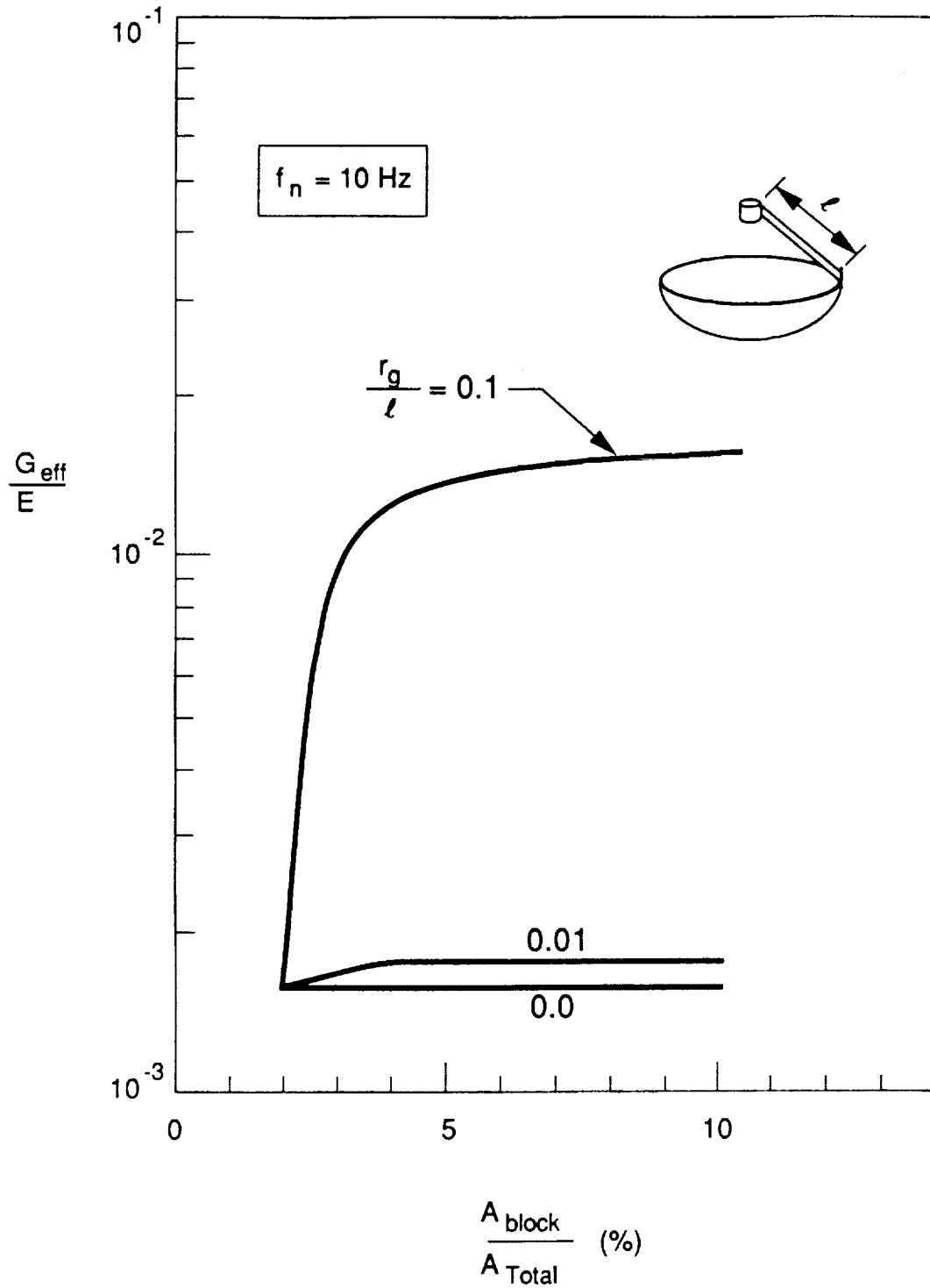


Figure 4-4. Minimum required G_{eff}/E to guarantee that f_n -torsion \geq f_n -bending for the cantilever configuration.

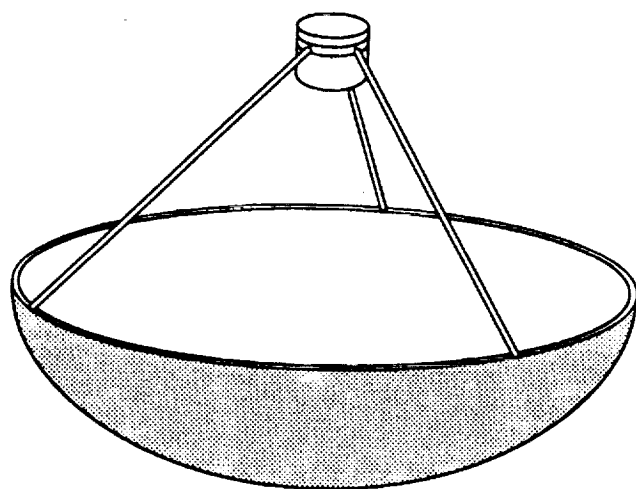


Figure 4-5. Rim-tripod configuration of feed support structure.

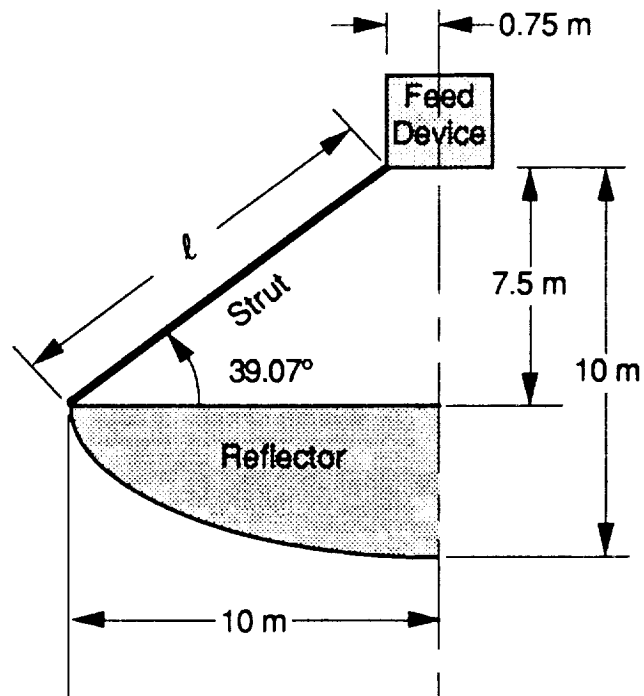


Figure 4-6. Rim-tripod FSS geometry - planar view through a single strut and reflector axis for the case $F/D = 0.5$ and $D = 20\text{m}$ (no scale).

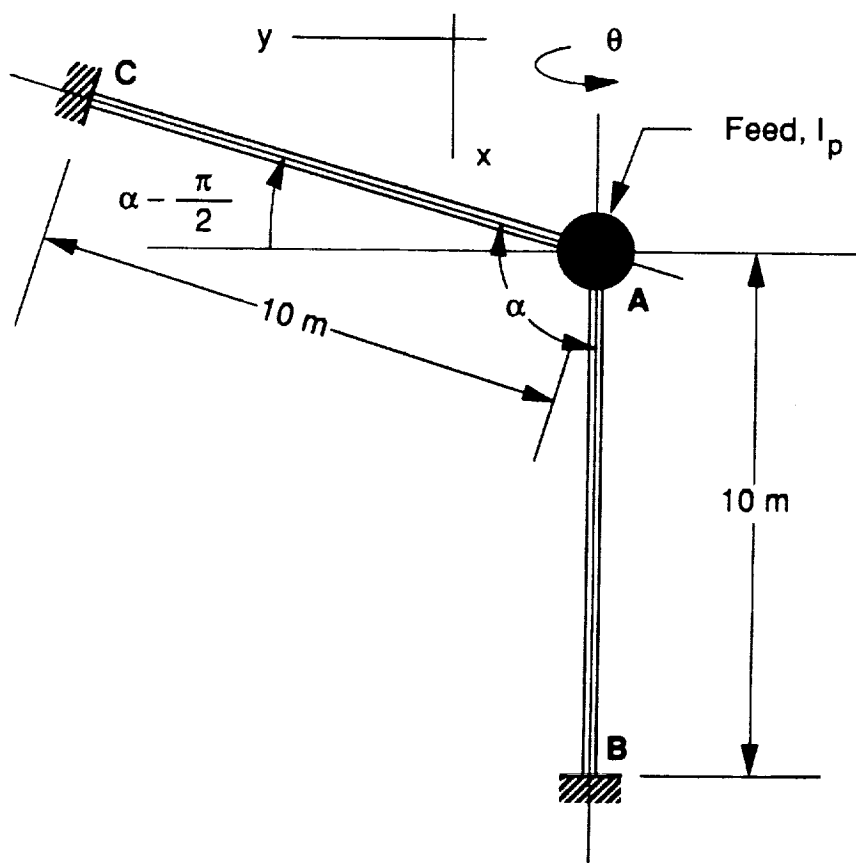


Figure 4-7. Planar view of tripod FSS with plane determined by centerlines of struts AB and AC. Axis of rotation is centerline of AB.

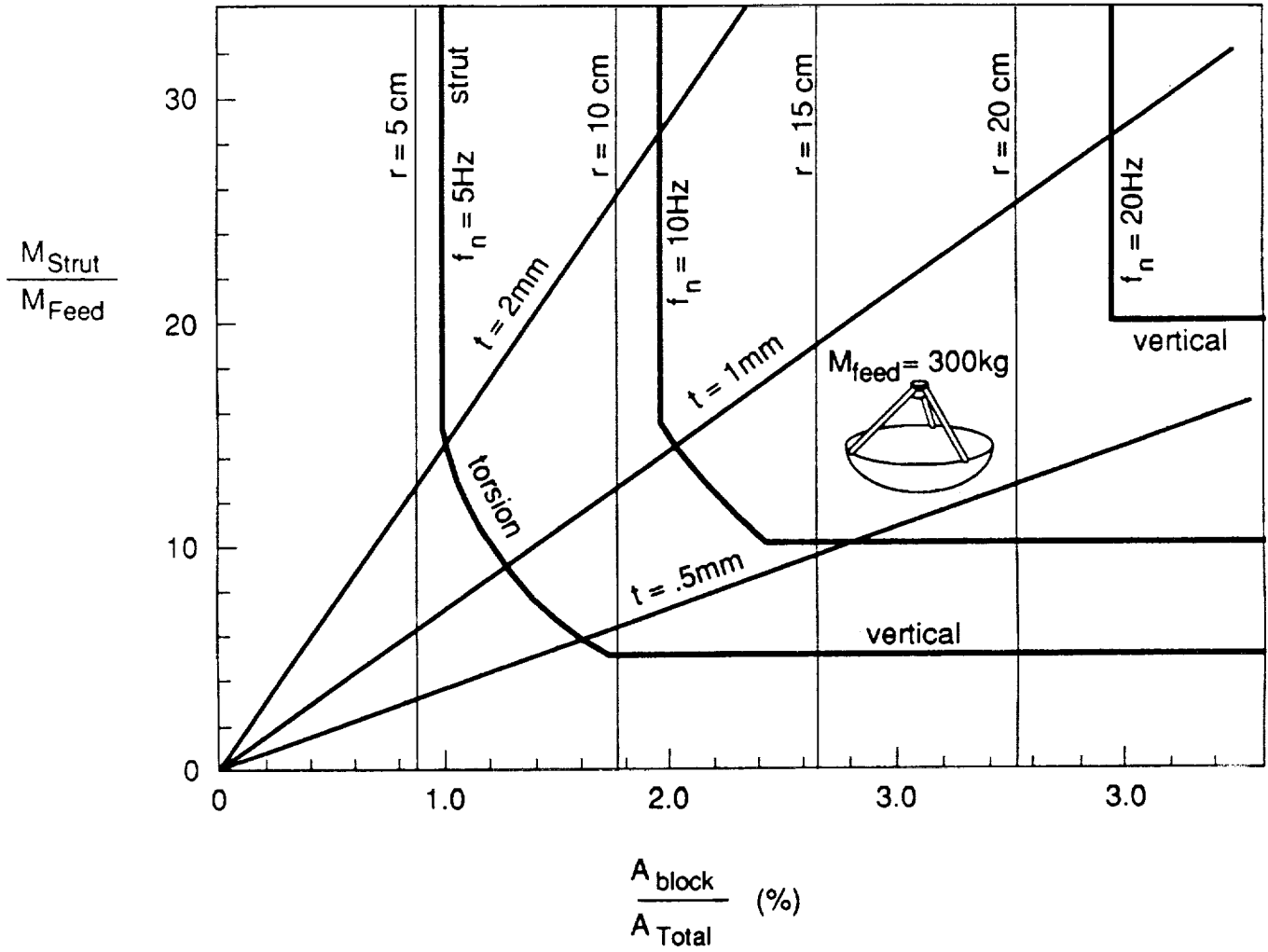


Figure 4-8. Feed support structure mass ratio (μ) versus assigned values of blocked area ratio, "a," fundamental, f_n , and radius of gyration, r_g , for the rim tripod configuration.

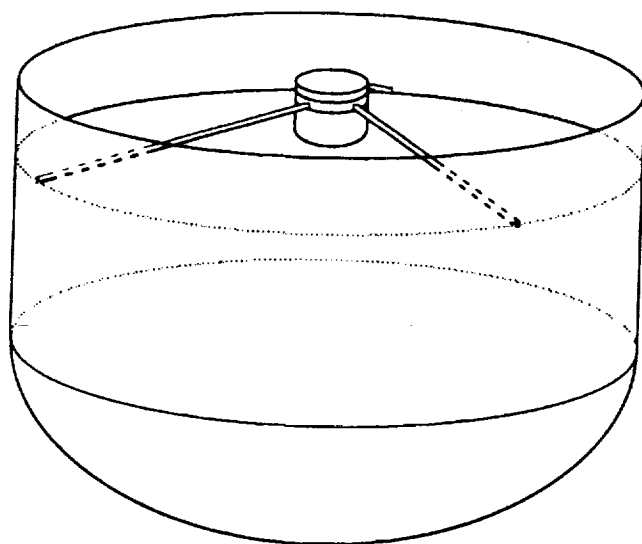


Figure 4-9. Sun shade- tripod configuration of feed support structure.

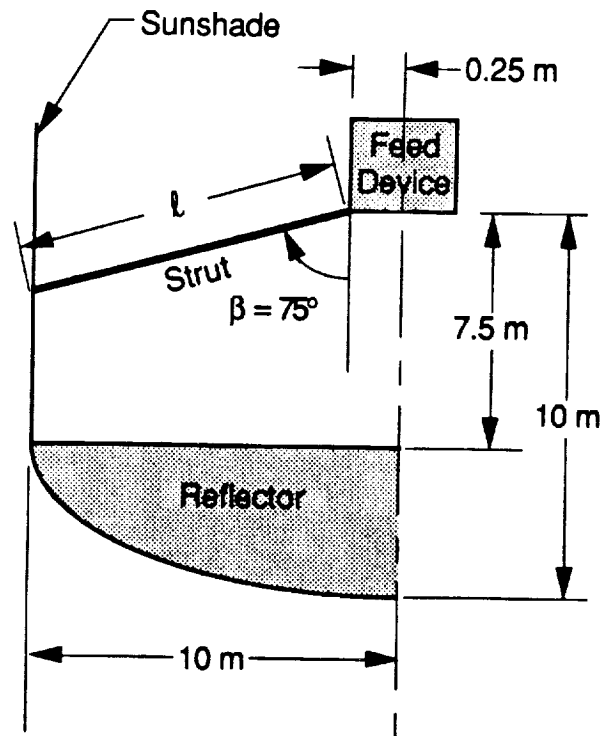


Figure 4-10. Sun shade-tripod FSS geometry - planar view through a single strut and reflector axis for the case $F/D = 0.5$ and $D = 20\text{ m}$ (no scale).

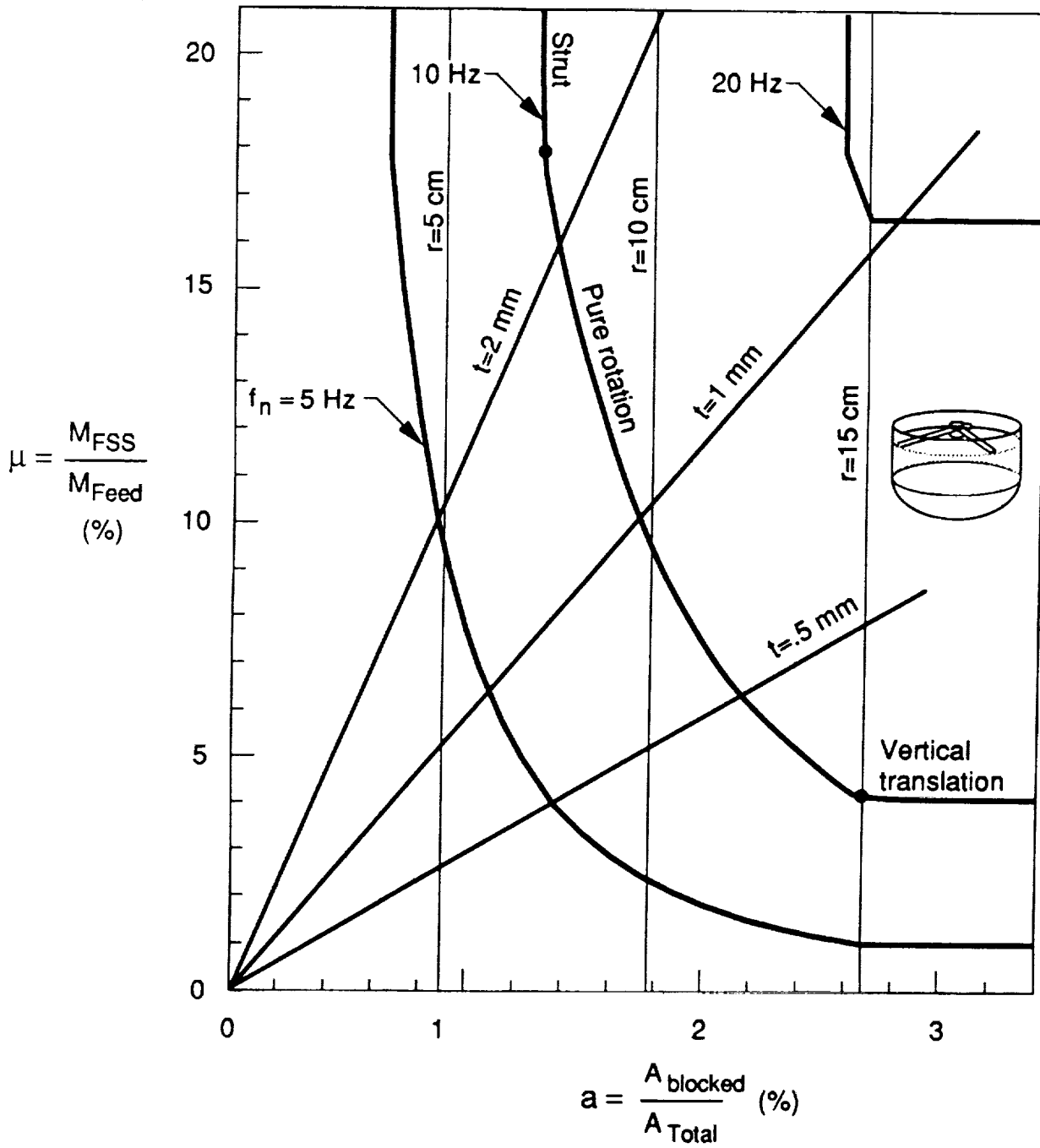


Figure 4-11. Structural mass ratio vs blocked area ratio for sunshade tripod configuration.

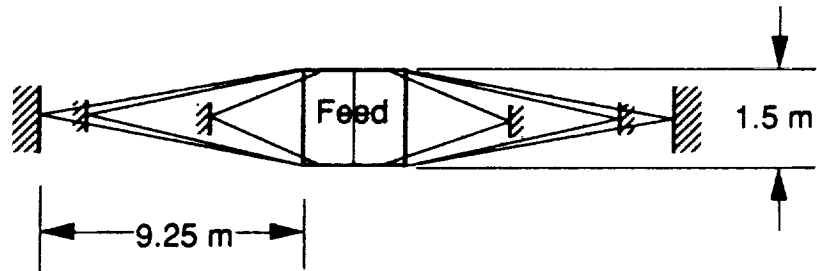
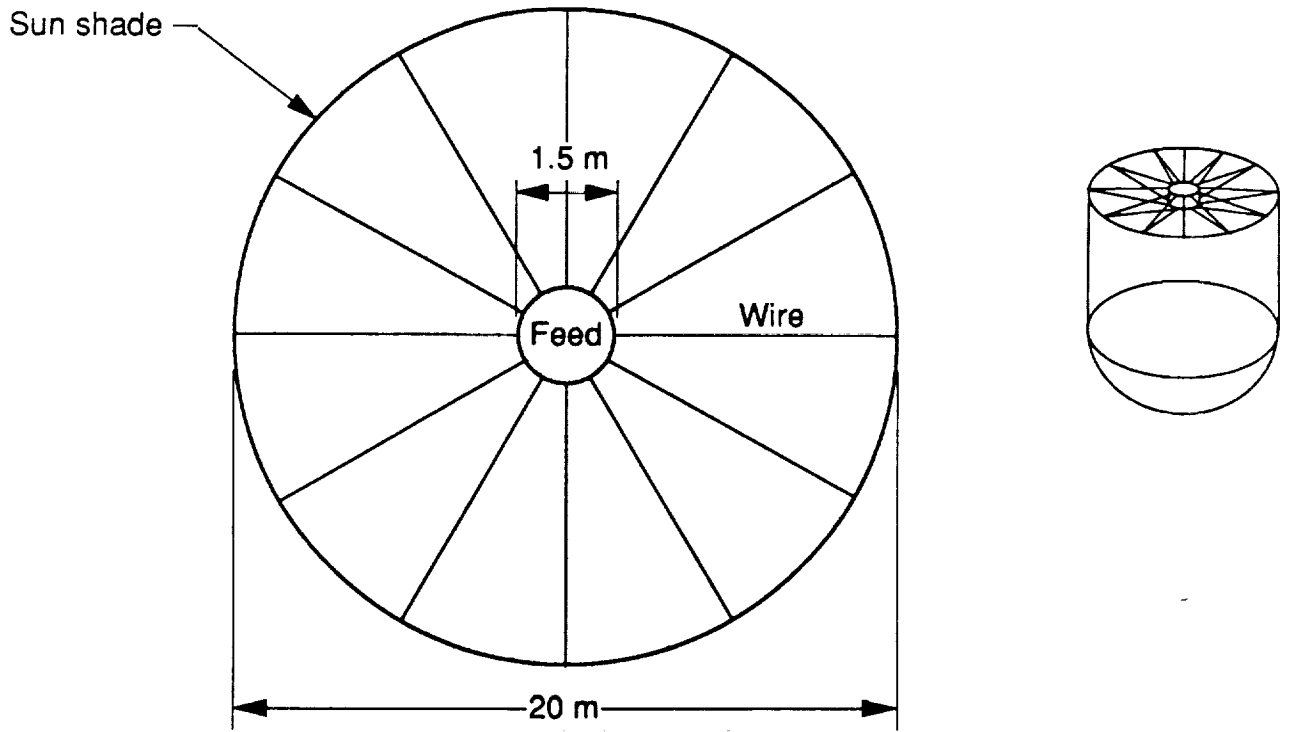


Figure 4-12. Radial spoke bicycle wheel configuration.

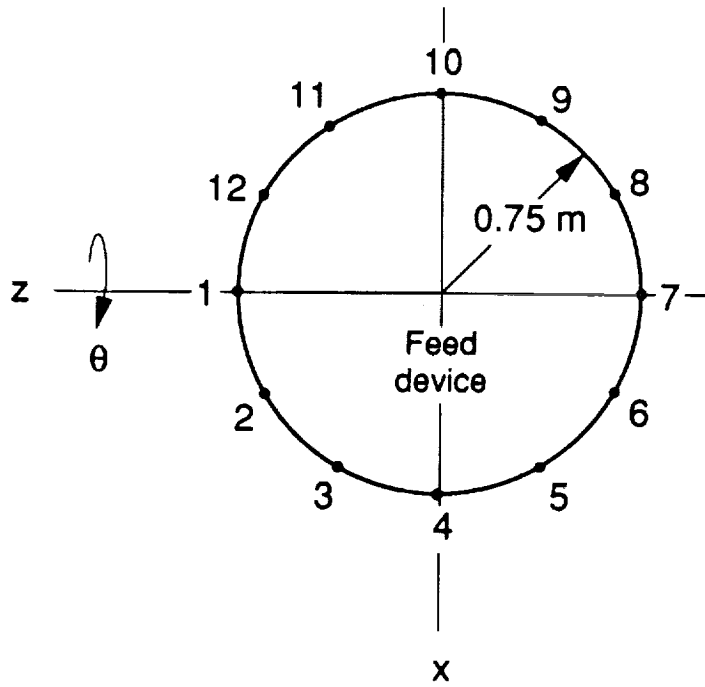


Figure 4-13. Geometry of pure rotation of feed device about an axis (Z) normal to reflector axis for RSBW configuration.

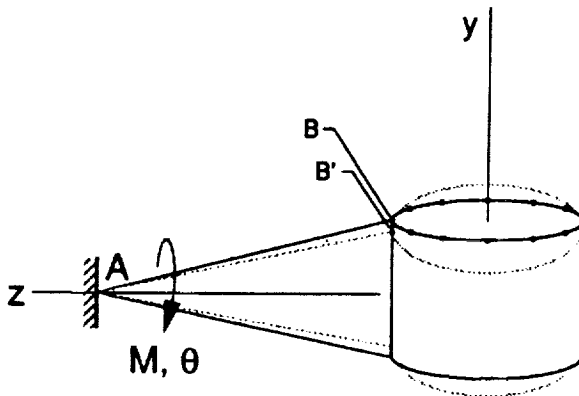


Figure 4-14. Geometry of torsional deformation of feed device about an axis (Z) normal to reflector axis for RSBW configuration.

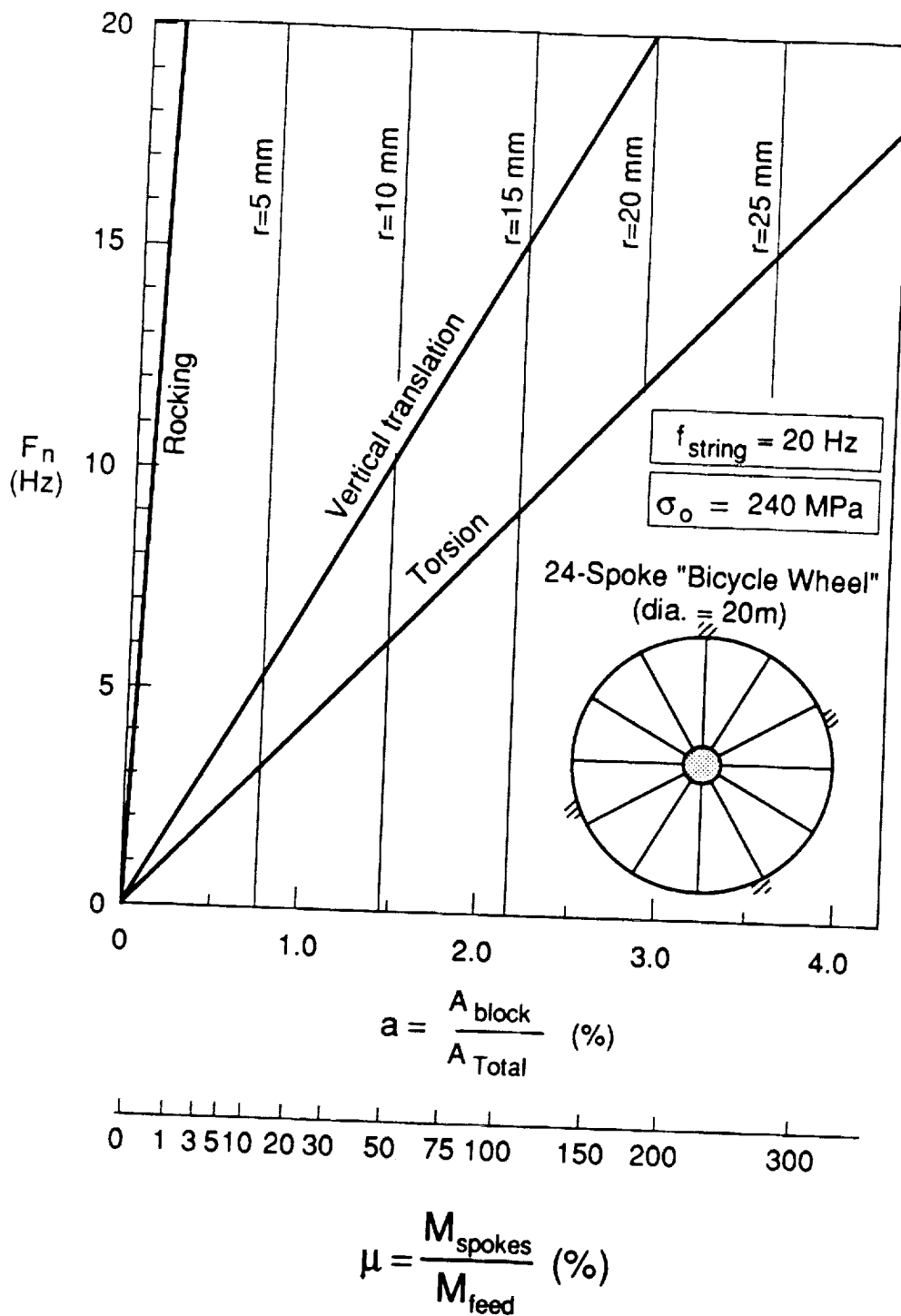


Figure 4-15. Dependence of fundamental frequency, f_n , for rocking vertical translation and torsion as functions of blocked area, "a", and mass ratio " μ ", radial spoke bicycle wheel configuration.

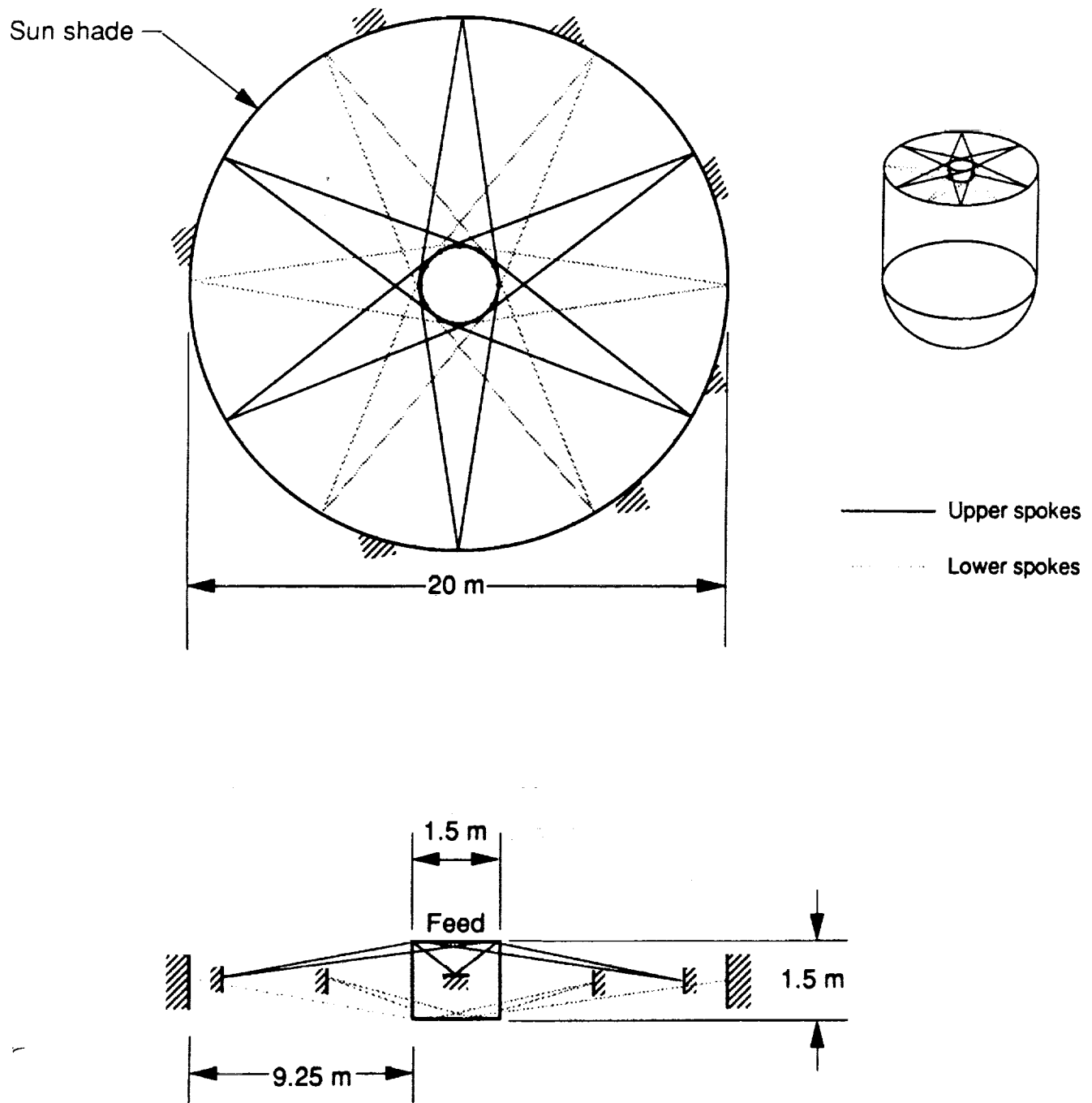


Figure 4-16. Interlaced spoke bicycle wheel (ISBW) configuration.

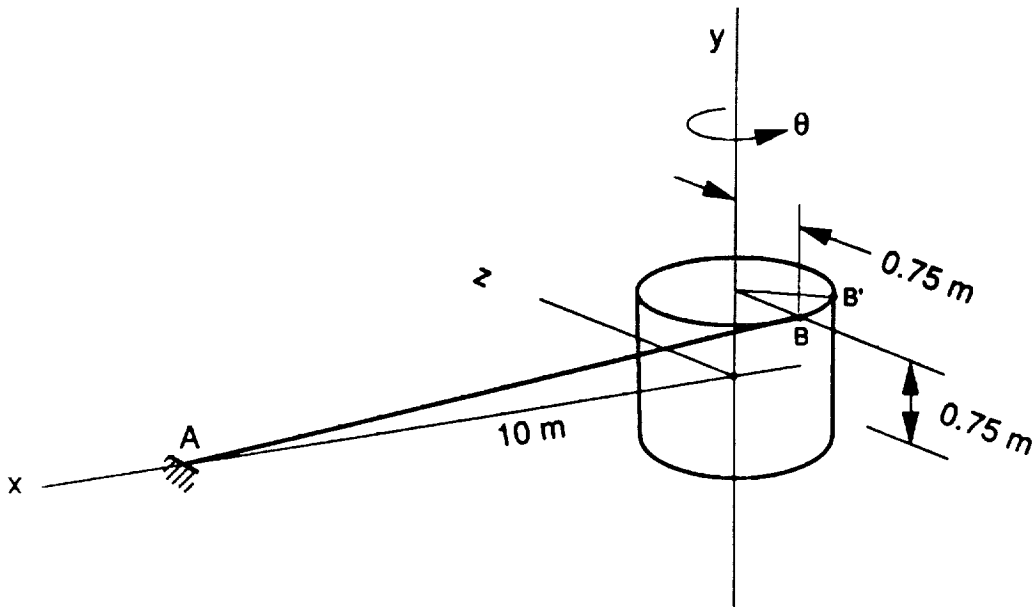


Figure 4-17. Geometry of deformation of spoke AB during torsional motion, ISBW configuration.

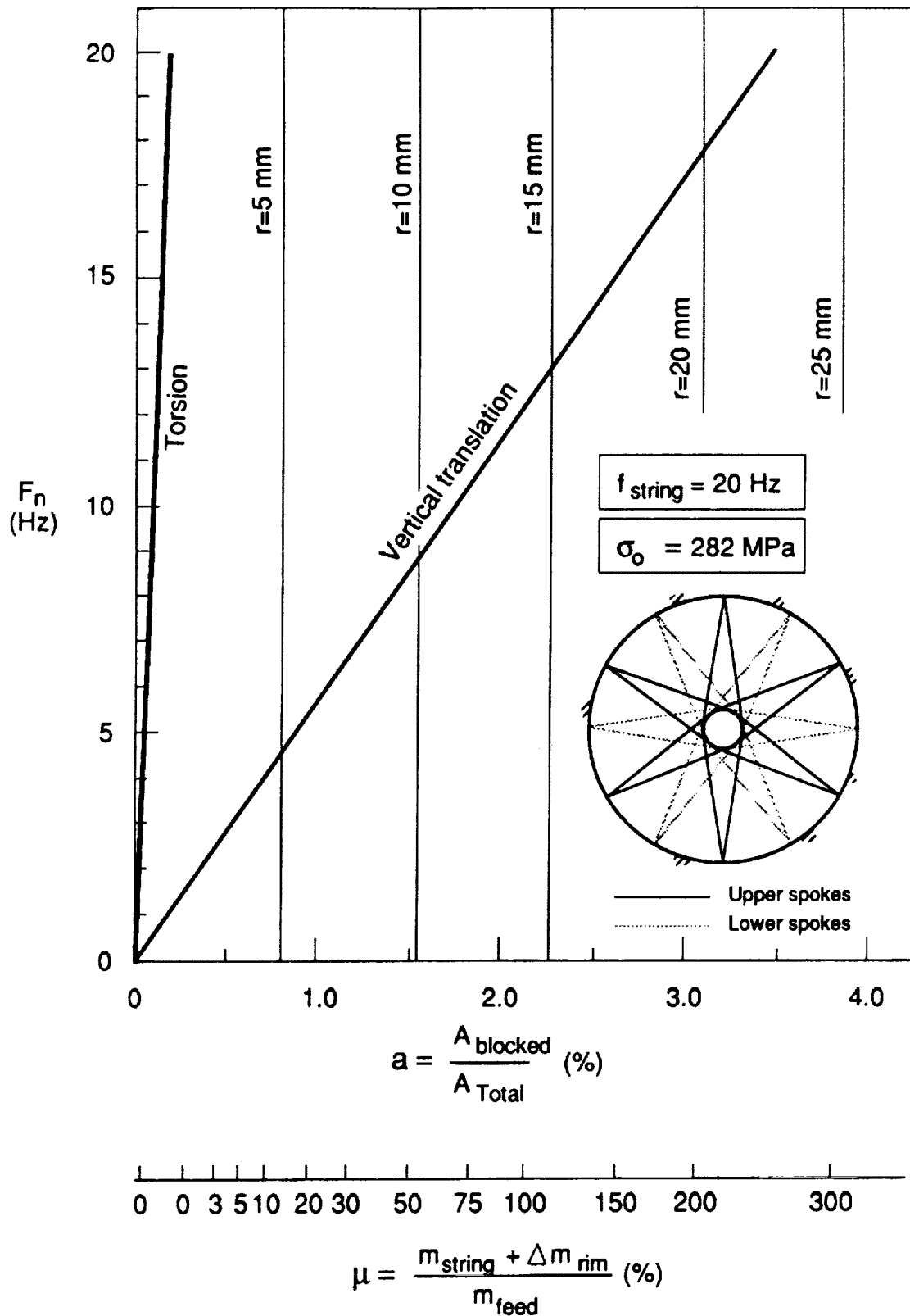


Figure 4-18. Fundamental frequency vs blocked area ratio and structural mass ratio for (ISBW) configuration.



Report Documentation Page

1. Report No. NASA CR-182064		2. Government Accession No.		3. Recipient's Catalog No.	
4. Title and Subtitle Concepts and Analysis for Precision Segmented Reflector and Feed Support Structures			5. Report Date December 1990		
			6. Performing Organization Code		
7. Author(s) Richard K. Miller, Mark W. Thomson and John M. Hedgepeth			8. Performing Organization Report No. AAC-TN-1157		
			10. Work Unit No. 506-43-41-02		
9. Performing Organization Name and Address Astro Aerospace Corporation 6384 Via Real Carpinteria, California 93013-2920			11. Contract or Grant No. NAS1-18567		
			13. Type of Report and Period Covered Contractor Report		
12. Sponsoring Agency Name and Address National Aeronautics and Space Administration Langley Research Center Hampton, Virginia 23665-5225			14. Sponsoring Agency Code		
			15. Supplementary Notes Langley Technical Monitor: W. B. Fichter Final Report - Task 3		
16. Abstract Several issues surrounding the design of a large (20-meter diameter) Precision Segmented Reflector are investigated. The concerns include development of a reflector support truss geometry that will permit deployment into the required doubly-curved shape without significant member strains. For deployable and erectable reflector support trusses, the reduction of structural redundancy was analyzed to achieve reduced weight and complexity for the designs. The stiffness and accuracy of such reduced member trusses, however, were found to be affected to a degree that is unexpected. The Precision Segmented Reflector designs were developed with performance requirements that represent the Reflector application. A novel deployable sunshade concept was developed, and a detailed parametric study of various feed support structural concepts was performed. The results of the detailed study reveal what may be the most desirable feed support structure geometry for Precision Segmented Reflector/Large Deployable Reflector applications.					
17. Key Words (Suggested by Author(s)) Large Deployable Reflector (LDR) Precision Segmented Reflector (PSR)			18. Distribution Statement Unclassified - Unlimited Subject Category 18		
19. Security Classif. (of this report) Unclassified		20. Security Classif. (of this page) Unclassified		21. No. of pages 90	22. Price A05

